Phosphorylation of luminal region of the SUN-domain protein Mps3 promotes nuclear envelope localization during meiosis

H. B. D. Prasada Rao[1], Takeshi Sato[2], Kiran Challa[3], Miki Shinohara[4], and Akira Shinohara*

Institute for Protein Research, Osaka University, Suita, Osaka 565-0871, Japan

Running head: Meiotic control of NE remodeling

Keywords: meiosis; CDK; DDK; Mps3; chromosome motion; Nuclear envelope (NE)

[1]Current address: National Institute for Animal Breeding, Hyderabad, India
[2]Current address: Kyoto Pharmaceutical University, Kyoto, Japan
[3]Current address: Friedrich Miescher Institute for Biomedical Research, Basel, Switzerland
[4]Current address: Graduate School of Agriculture, Kindai University, Nara, Japan

*Correspondence:
Akira Shinohara
Institute for Protein Research, Osaka University
3-2 Yamadaoka, Suita, Osaka 565-0871, Japan
Telephone: 81-6-6879-8624
FAX: 81-6-6879-8626
E-mail: ashino@protein.osaka-u.ac.jp
ORCID: 0000-0003-4207-8247

Summary

During meiosis, protein ensembles in the nuclear envelope (NE) containing SUN- and KASH-domain proteins, called linker nucleocytoskeleton and cytoskeleton (LINC) complex, promote chromosome motion. How LINC complexes acquire the meiotic property is largely unknown. Here we showed that cyclin-dependent protein kinase (CDK) and Dbf4-dependent Cdc7 protein kinase (DDK) promote proper meiosis-specific localization of yeast SUN-domain protein Mps3 on NE and control force-dependent movement of chromosomes during meiosis. We also found a NE luminal region of Mps3 juxtaposed to inner nuclear membrane (INM) is required for meiosis-specific localization of Mps3 on NE. Negative charges introduced by meiosis-specific non-canonical phosphorylation of the luminal region of Mps3 changes its interaction with INM, which may induce NE localization by promoting the formation of a canonical LINC complex with Mps3. Our study reveals unique phosphorylation-dependent regulation on the localization and function of Mps3 protein in meiotic NE remodeling.

Introduction

During meiosis, homologous chromosomes pair with each other. This pairing leads to juxtaposition of the chromosomes along their entire length, resulting in the formation of the synaptonemal complex (SC). SC is a proteinaceous structure comprising two chromosome axes called the axial/lateral element (AE/LE) flanking a central region with a ladder-like structure (Hawley and Gilliland, 2009; Zickler and Kleckner, 1999). AE formation is initiated in the leptotene stage of meiotic prophase I, accompanied with the assembly of the chromosome axis with multiple chromatin loops. In the zygotene stage, a part of homologous AE pairs each other to form a short SC. In the pachytene stage, SC is elongated along the entire chromosome. After the pachytene stage, SC dismantles in the diplotene stage before the onset of meiosis I.

Meiotic cells also exhibit a unique arrangement of chromosomes inside of the nucleus. In most organisms, telomeres attach to nuclear envelopes (NEs) in early meiotic prophase (or premeiotic phase) and occasionally cluster on one area of NE, particularly near the vicinity of the centrosome (a microtubule organizing center) (Zickler and Kleckner, 1998). Telomere clustering is seen in only the zygotene stage and is known as “telomere/chromosome bouquet.” In the pachytene stage, telomere bouquets are resolved and telomeres are dispersed over the entire NE. The bouquet configuration of chromosomes is proposed to promote homologous pairing by restricting the homology search process from three dimension to two dimension (Zickler and Kleckner, 1998).

Recent studies revealed the very dynamic nature of meiotic chromosomes in various organisms from yeasts to mammals (Hiraoka and Dernburg, 2009; Koszul and Kleckner, 2009). The oscillated motion of a nuclei during meiotic prophase I has been well described in fission yeast (Chikashige et al., 2007). The nuclear movement is driven by cytoplasmic microtubule cables, along which SPB embedded in NE moves together with clustered telomeres. This telomere-led movement promotes pairing of homologous loci on chromosomes. Although less coordinated, chromosome motion throughout prophase I has been reported in budding yeast, nematodes, maize and mouse (Penkner et al., 2009; Sato et al., 2009a; Sheehan and Pawlowski, 2009).

Protein ensembles embedded in NE that connect telomeres in nucleoplasm with the cytoskeleton in cytoplasm, which are referred to as the LINC (linker of nucleocytoskeleton and cytoskeleton) complex, promote meiotic chromosome motion (Hiraoka and Dernburg, 2009; Starr and Fridolfsson, 2010). The LINC complex necessary for chromosome motion contains an inner nuclear membrane (INM) protein harboring the SUN (Sad1/UNc-84) domain and an outer nuclear membrane (ONM) protein with the KASH (Klarsicht, ANC-1, SYNE1 Homology) domain. SUN and KASH domains interact with each other in a space between INM and ONM, luminal region or peri-nuclear space. SUN-domain proteins bind to telomeres and/or nucleocytoskeleton in nucleoplasm while KASH-domain proteins bind to cytoskeletons. LINC complexes transmit forces generated by cytoskeleton to NEs for nuclear positioning and migration in somatic cells and to telomeres for chromosome motion in meiotic cells (Starr & Fridolfsson 2010).

In *Saccharomyces cerevisiae*, telomeres are tethered to NEs as several clusters during mitosis and move around NEs during meiotic prophase I. These telomeres are transiently clustered during prophase I (Conrad et al., 2008; Koszul et al., 2008; Trelles-Sticken et al., 2000; Trelles-Sticken et al., 1999). Telomere movement on NE drives chromosome motion inside the nucleus (Koszul et al., 2008; Scherthan et al., 2007). At least three distinct regulatory steps facilitate chromosome motion in the budding yeast meiosis. First, meiosis-specific components of the LINC complex, such as Ndj1 and Csm4, are expressed and incorporated. Ndj1 is a meiosis-specific telomere-binding protein necessary for telomere tethering to NEs (Chua and Roeder, 1997; Conrad et al., 1997), whereas Csm4 is a meiosis-specific ONM protein (Conrad et al., 2007; Kosaka et al., 2008; Wanat et al., 2008), which interacts with a unique class of KASH protein, Mps2 (Chen et al., 2019; Lee et al., 2020). Second, the formation of actin cables is specifically induced in the cytoplasm of meiotic cells (Koszul et al., 2008; Taxis et al., 2006). Third, NE dynamics including NE remodeling and movement occur prominently in meiotic prophase I (Conrad *et al.* 2007; this paper). NE remodeling is accompanied by NE localization of a yeast SUN-domain protein, Mps3/Nep98 (Conrad et al., 2007) as well as Mps2 (Lee et al., 2020). In mitosis,

Mps3 and Mps2 predominantly localizes to SPB as a component of the half-bridge as well as SPB-interacting network (SPIN) (Chen et al., 2019) and play an essential role in SPB duplication (Jaspersen et al., 2002; Nishikawa et al., 2003). During meiotic prophase-I, in addition to SPB, Mps3 localizes as a distinct protein ensembles on NE as a LINC complex (Conrad et al., 2007). In early meiotic prophase I, Mps3 forms several distinct foci/patches on NE and later shows more disperse staining around NE. Mps3 plays an important role in telomere/chromosome dynamics (Conrad et al., 2007). However, how meiosis-specific Mps3 localization on NE is induced is poorly understood.

Here we showed that cyclin-dependent Cdc28 kinase (CDK) and Dbf4-dependent Cdc7 kinase (DDK) are necessary for proper telomere movement, particularly for the resolution of telomere clusters. Defects in telomere movement induced by CDK- and DDK-inactivation are associated with impaired meiosis-specific NE localization of Mps3; resolution of Mps3 clusters. We also found that a luminal region of Mps3, which is located near INM, is important for its NE localization. This region is subject to phosphorylation during meiosis prophase I. Phospho-defective *mps3* mutant protein showed reduced NE localization during meiosis. Introduction of negative charged residues in this region suppresses the defects in Mps3 localization in *cdk* and *ddk* mutants. In reconstituted liposomes, a Mps3 peptide containing the luminal region with negatively charged residues showed reduced affinity to the membrane relative to a control wild-type Mps3 peptide. Our results suggested that collaborative action of CDK and DDK and Mps3 luminal region control Mps3 localization to NE, thus, the assembly of meiosis-specific canonical LINC complex for chromosome motion and NE remodeling during meiosis.

Results

Force-independent localization of Mps3 on NE during meiosis

We examined the localization of Mps3-GFP (Conrad et al., 2007) in various mutants. Mps3-GFP showed stage-specific distribution and movement on NE (Figure 1A, 1B). During meiotic prophase I, Mps3 shows unique localization patterns on NE. At 0 h, Mps3 predominantly localizes on SPB as a single focus on NE (Figure 1A) (Jaspersen et al., 2002; Nishikawa et al., 2003) with little movement (Figures 1A, 1C). During early prophase I including meiotic S phase (2–3 h), Mps3 formed 2–5 foci (including 1 focus in SPB) on NE with slow movement. After 3 h, the number of Mps3 foci increased to more than 5, and several Mps3 foci fused to form a patch (Figures 1A-1D), as shown previously (Conrad et al., 2007). During this stage, Mps3 foci/patches moved around NE with oscillated motion (Figure 1C). At 3-5 h, some Mps3 foci/patches localized to one area of NE with clustering. In late prophase I (e.g., at 5 and 6 h), Mps3 often covered most parts of NE and was associated with NE deformation and protrusion (Figure 1). These localizations were classified in four classes and quantified at each time point (Figure 1B). After 6 h, most Mps3 signals on NE disappeared, leaving two SPB-associate foci (Figure 1A).

Although Mps3 movement was dependent on Cms4 and partly on Ndj1 (Chua and Roeder, 1997; Conrad et al., 1997) (Conrad et al., 2007; Kosaka et al., 2008; Wanat et al., 2008), Mps3 localization on NE did not depend on Ndj1 and Csm4 (Figure 1D). At late times such as 5 h, the *ndj1* mutant showed full coverage of Mps3 on NE (Conrad et al., 2007) with NE deformation (distorted nucleus) and motion. The *csm4* mutant formed multiple Mps3 patches/foci on NE (Conrad et al., 2007; Kosaka et al., 2008; Wanat et al., 2008), but did not show complete coverage on NE with multiple foci/patches. The *csm4* mutant is also defective in clustering and motion of Mps3 foci/patches as well as NE deformation (with round nucleus). Moreover, we examined the effect of an actin polymerization inhibitor, latrunculin B (LatB), on Mps3 localization (Trelles-Sticken et al., 2005). Treatment of meiotic cells with LatB, that disrupted the cytoplasmic actin cables but not the actin patches (Figure S1B), showed normal distribution of Mps3 foci/patches on NE during prophase (Figure 1D). However, as shown previously

176 (Trelles-Sticken et al., 2005), dynamic movement of Mps3-GFP was completely
177 absent (Figure 1D) without deformation of nuclei. These defects are similar to
178 those in the *csm4* mutant. At one-hour after washing out LatB, the motion of Mps3
179 resumed. These results suggested that Mps3 dynamics during meiosis can be
180 functionally separated into two processes: force-independent NE localization and
181 force-dependent motion. The force-dependent motion requires actin
182 polymerization and Csm4, and party Ndj1. On the other hand, the force-
183 independent NE localization does not require action polymerization or Csm4
184 (Ndj1), suggesting unique localization mechanism of Mps3 on NE during meiosis.
185

186 **CDK and DDK promote efficient Mps3 localization on NE during meiosis**

187 Because Mps3-dependent telomere movement is initiated in early meiotic
188 prophase (Conrad et al., 2008; Koszul et al., 2008; Trelles-Sticken et al., 2000;
189 Trelles-Sticken et al., 1999), we analyzed the role of two protein kinases that are
190 active from early meiosis; CDK and DDK. Because CDK and DDK are essential
191 for vegetative growth, we used conditional mutant alleles of the catalytic subunits
192 of CDK and DDK (Cdc28 and Cdc7), *cdc28-as1* and *cdc7-as3*, which are
193 sensitive to specific inhibitors,1NM-PP1 and PP1, respectively (Benjamin et al.,
194 2003; Wan et al., 2006). Although CDK and DDK are also essential for DNA
195 replication and recombination in meiosis, telomere movement during meiosis,
196 thus Mps3 dynamics, is independent of replication and recombination (Trelles-
197 Sticken *et al.* 1999; Trelles-Sticken *et al.* 2000).

198 We performed time-lapse analysis of Mps3-GFP in the *cdc28-as1* and *cdc7-*
199 *as3* in either absence or present of each specific inhibitor. To inactivate CDK,
200 1NM-PP1, that did not affect Mps3-GFP dynamics in wild-type cells (Figure S1A),
201 was added to the *cdc28-as1* at 0h. In the absence of the inhibitor, the mutant cells
202 showed normal Mps3 localization during meiosis (Figure 1E). CDK inactivation
203 induced impaired Mps3 localization (Figures 1B, 1E). We detected a few Mps3
204 foci/patches, which clustered on one area of NE. These loose clusters of Mps3
205 patches were persistent during prophase I (Figures 1B). On the other hand, upon
206 CDK inhibition, the formation of multiple Mps3 foci/patches around NE and fully
207 coverage of Mps3 on NE was largely diminished. Tracking motion of Mps3 foci
208 showed persistent clustering with restricted motion of the foci on one region of

209 NE under the condition (Figure 1F). Importantly, at 2 h after washing the inhibitor,
210 NE localization and motion of Mps3 was recovered. CDK inactivation after meiotic
211 S phase (the addition of the inhibitor at 3 h) interfered with disperse localization
212 of Mps3 throughout NE with loose clustering of Mps3 foci/patches. Therefore,
213 persistent CDK activity is necessary for the establishment and maintenance of
214 Mps3 disperse localization, particularly the resolution of clustering, and normal
215 movement on NE.

216 A similar defect in Mps3 localization on NE and movement was observed
217 with DDK inactivation (*cdc7-as3* + PP1) (Figure 1B, 1E). PP1 did not affect the
218 localization of Mps3-GFP in wild-type cells (Figure S1A). In its absence, the *cdc7-*
219 *as3* cells showed normal localization and motion of Mps3 foci/patches (Figures
220 1B, 1E). DDK inhibition by PP1 from 0 h reduced NE localization of Mps3 with
221 accumulation as a loose cluster at late meiosis. Removal of the inhibitor restored
222 the NE localization of Mps3 in the *cdc7-as3* cells. The addition of PP1 at 3 h also
223 induced similar Mps3 localization defect to that at 0 h. Although CDK and DDK
224 are essential for pre-meiotic DNA replication and DSB formation, the inactivation
225 of either kinase after the DNA replication and DSB formation resulted in the
226 impaired localization, suggesting direct regulatory role of these kinases in Mps3
227 dynamics. Moreover, the defect in Mps3 localization under DDK inactivation is
228 similar to that under CDK inactivation, suggesting that CDK and DDK work in a
229 same pathway to control Mps3 dynamics during meiosis.

230 We also analyzed the Mps3-GFP localization in the *cdc7 bob-1-1* double
231 mutant, in which the *bob1-1* mutation in the helicase gene *MCM5* suppresses the
232 lethality of *cdc7* deletion (Jackson et al., 1993; Sasanuma et al., 2008), A small
233 fraction (~20%) of the *cdc7 bob-1* mutant cells showed a few Mps3 foci on NE
234 while the most of cells did not form some Mps3 foci on NE. These defect in the
235 *cdc7 bob-1-1* double mutant is more severe than that in the *cdc7-as3* mutant with
236 PP1. Whole cell immunostaining of the Mps3-Flag protein showed that reduced
237 CDK and DDK activities hampered localization of Mps3, but not of Ndj1, to NE
238 during meiosis (Figure 1G), suggesting a critical role of the kinases in the coupling
239 of Mps3 to Ndj1 on NE, suggesting Mps3-independent pathway for Ndj1
240 localization on NE. Taken together, these results revealed that CDK and DDK
241 activities are necessary for proper Mps3 localization and efficient movement on

242 NE during meiosis.
243
244 **CDK and DDK promote telomere dynamics during meiosis**
245 To know the role of CDK and DDK in telomere movement, we analyzed the motion
246 a green fluorescent protein (GFP) fusion of a telomere-binding protein, Rap1, as
247 described (Conrad et al., 2008; Koszul et al., 2008; Trelles-Sticken et al., 2000;
248 Trelles-Sticken et al., 1999). During vegetative growth or pre-meiosis, Rap1-GFP
249 exhibited 1–4 foci on NE on a single focal plane with little movement (Figure 2A)
250 (Trelles-Sticken et al., 2005). Once the cells entered meiosis, Rap1 foci on NE
251 increased in number (up to 10). Rap1-GFP foci moved rapidly and were
252 occasionally clustered in a single area of NE (Figure 2A), which corresponds to
253 the telomere bouquet (Trelles-Sticken et al., 2005). This telomere clustering was
254 very transient (half-life less than 5 second) and was predominantly observed after
255 3–4 h of incubation in a sporulation medium (Figures 2A, 2E). Rap1 foci were
256 more dispersed during late meiotic prophase (4–6 h for the pachytene stage)
257 before the onset of meiosis I (MI; Figure 2A). The tracking analysis showed that
258 Rap1 foci move around a meiotic nucleus in an uncoordinated way as reported
259 (Figure 2D) (Trelles-Sticken et al., 2005).
260 CDK inactivation (*cdc28-as1* + 1NM-PP1) impaired meiotic Rap1
261 dynamics (Figures 2B, 2E). The *cdc28-as1* showed normal Rap1 dynamics
262 during meiosis (Figures 2B, 2E). With compromised CDK activity from 0 h, cells
263 with clustered Rap1 foci accumulated during prophase I (Figure 2E). A few Rap1
264 foci or patches showed polarized localization on one peripheral area of a nucleus.
265 indicating that CDK activity is required for meiotic telomere dynamics, particularly
266 for the resolution of telomere clusters (but not necessarily for clustering *per se*).
267 The 2D tracking confirmed the restricted motion of Rap1 foci in one nuclear area
268 (Figure 2D). Addition of an inhibitor during early prophase I (e.g., at 3 h) also
269 resulted in defective resolution of telomere clustering; washing off the inhibitor
270 restored telomere dynamics (Figure 2B). Treatment of wild-type cells with the
271 inhibitor did not affect Rap1-GFP dynamics, confirming the specificity of the
272 inhibitor (Figure S1C). These results indicated that persistent CDK activity during
273 meiotic prophase I promotes normal telomere dynamics. The inactivation of CDK,
274 which regulates actin dynamics in mitotic cells, does not affect the formation of

275 cytoplasmic actin cables during meiosis (Figure S2A).

276 Similar to CDK inactivation, Cdc7 inactivation (the treatment of the *cdc7-*
277 *as3* with PP1) at 0 and 3 h impaired Rap1-GFP dynamics, which showed
278 accumulation of clusters with limited motion (Figures 2C, 2E); whereas the
279 treatment of the wild-type cells with PP1 did not affect Rap1 dynamics (Figure
280 S1C). This defective resolution of Rap1 cluster under DDK inhibition is similar to
281 that seen in CDK inhibition. Moreover, the *cdc7* null mutant with *bob1-1* mutation
282 exhibited persistent telomere clustering (Figures 2C, 2D, 2E). These results
283 indicated that persistent Cdc7 kinase activity is also required for meiotic telomere
284 dynamics.

285

286 **Mps3 is phosphorylated during meiosis**

287 Previously, it is shown that S70 of Mps3 is phosphorylated in late prophase-I (Li
288 et al., 2017). We also found that Mps3 is a phosphoprotein in middle prophase I.
289 On western blots, Mps3-Flag showed mobility shift, which is induced during
290 meiotic prophase I (4 and 6 h; Figure 3C). Mps3 mobility was reduced by the
291 treatment with a lambda phosphatase (Figure S2B). Moreover,
292 immunoprecipitation (IP) of Mps3-Flag from meiotic cells showed that Mps3
293 cross-reacted with anti-phosphoserine antibody (Figure S2C) whose reactivity
294 was largely diminished by treatment with the phosphatase.

295 Previous systematic analyses of CDK substrates *in vitro* identified Mps3
296 as a Cdc28–Clb2 substrate (Ubersax et al., 2003). Mps3 contains five potential
297 CDK sites (S/TPXK/R or S/TP), two of which seem to be candidates for CDK/DDK
298 phosphorylation (188–190 <u>TSS</u>PGK and 450–451 <u>TS</u>P; Figure 2A, S2A).
299 Because the 450–451 site is located in the SUN domain, which is not essential
300 for Mps3 localization on NE (Rao *et al.* 2011), we focused on T188-S189-S190
301 (hereafter, TSS; Figure 3B). We purified a GST fusion protein of an Mps3
302 fragment (residue 160–260) including TSS. *In vitro* Cdc28–Clb5 alone, but not
303 Cdc7–Dbf4 alone, promoted phosphorylation of the Mps3 fragment
304 (approximately 10-fold compared to the background; Figure S3E). Co-incubation
305 with CDK and DDK resulted in robust incorporation of ^{32}P in GST-Mps3, indicating
306 that CDK and DDK cooperate in Mps3 phosphorylation *in vitro* (30-fold compared
307 to the background). Triple alanine substitutions (T188A, S189A, S190A; referred

308 to as the *mps3-AAA* mutant) made the GST-Mps3 fragment a poor substrate by
309 these kinases. These results indicated that TSS is required for efficient CDK/DDK
310 phosphorylation *in vitro*.
311 Consistent with the *in vitro* result, the Mps3-AAA mutant protein showed a
312 reduced band shift and decreased reactivity to anti-phosphoserine antibody
313 (Figures 3C and S3F). Furthermore, we raised an antibody against a Mps3
314 peptide with 189-phosphoserine and 190-phosphoserine (186-
315 GAT**pSpS**PGKSF-195) and found that this phospho-specific antibody could
316 recognize immunoprecipitated Mps3-Flag specifically between 4–8 h in meiosis,
317 but not in mitosis (Figure 3D). Strong signals were observed during late prophase
318 I (4 and 6 h). This antibody did not recognize precipitated Mps3-AAA-Flag. These
319 results indicate that 189S and 190S are phosphorylated *in vivo* specifically during
320 meiosis.
321 Accidently, the Mps3 sequence around putative phosphorylation sites is
322 similar to that with phosphorylation sites on Mer2 (Henderson et al., 2006;
323 Sasanuma et al., 2008; Wan et al., 2008), including TSSP sequence (Figure 3B).
324 Mer2 is a meiosis-specific protein essential for DSB formation (Cool and Malone,
325 1992; Engebrecht et al., 1990). CDK and DDK phosphorylate the TSS sequence
326 of Mer2, which are necessary for meiotic DSB formation. We swapped a 10-
327 amino-acid region (GATSSPGKSF) containing the Mps3 phosphorylation sites
328 with the corresponding region of Mer2 (TETSSPFRST; Figure 3B). This *MPS3*
329 allele (*MPS3-MER2S*) conferred wild-type spore viability (95%; n=50 tetrads).
330 The *MPS3-MER2S-Flag* exhibited similar telomere (Rap1) clustering to the wild
331 type (Figures 3F and 3G). The Mps3-MER2S protein cross-reacted with
332 antibodies against Mer2 phospho-S30 antibody (Henderson *et al.* 2006), but not
333 with the anti-Mps3-phospho antibody (Figures 3D and 3E). The Mps3-MER2S-
334 Flag protein shows meiosis-specific localization on NE which often co-localized
335 with Ndj1 (Figure 3H). These suggest that residues 26-35 of Mer2 are functionally
336 equivalent to residues 185-194 of Mps3. Like Mps3, the region of Mer2 is rich in
337 serine and threonine (Figure 3B).
338
339 **The *mps3-AAA* mutant is defective in Mps3 localization on NE**
340 To investigate the role of the phosphorylated residues of Mps3, we constructed

341 and characterized phenotypes of the *mps3-AAA-FLAG* mutant (hereafter, *mps3-*
342 *AAA*; Figure 4). The *mps3-AAA* mutant showed little apparent defects in mitosis
343 such as SPB duplication (Figure S3A) seen in other *mps3* mutants (Jaspersen et
344 al., 2002; Nishikawa et al., 2003), suggesting that TSS residues of Mps3 are not
345 critical for the mitotic function of Mps3. The *mps3-AAA* mutant showed defects in
346 meiosis with reduced spore viability of 87.5%, which is slightly higher than that of
347 the *ndj1* mutant (75.8%) (Chua and Roeder, 1997; Conrad et al., 1997). The
348 spore viability of the *ndj1 mps3-AAA* double mutant is 72.3%, which is similar to
349 that of the *ndj1* mutant. The *mps3-AAA* mutant delayed the entry to meiosis I by
350 ~1 h relative to the wild type (Figure 4A). The *ndj1 mps3-AAA* double mutant
351 showed ~2.5 h delayed entry into meiosis I, which is similar to the *ndj1* single
352 mutant, indicting the epistatic relationship of the *mps3-AAA* to the *ndj1*. The
353 *mps3-AAA* mutant shows normal progression of meiotic S-phase (Figure S3B).
354 Immuno-staining of Zip1, a component of central region of SC, revealed delayed
355 formation of full length SCs together in the *mps3-AAA* mutant with delayed
356 loading of Zip1 at early time points (Figures S3C, S3D), suggesting that Mps3 NE
357 localization is necessary for efficient synapsis.
358 We also analyzed chromosome dynamics during meiosis of the *mps3-AAA*
359 mutant cells. First, we checked Rap1-GFP movement in the *mps3-AAA* mutant.
360 Different from the wild-type cells, the *mps3-AAA* mutant was defective in
361 movement of Rap1-GFP and, thus of telomeres (Figures 4B,4C). In the mutant,
362 the number of Rap1 foci did not increase (Figure 4B) and little movement of Rap1-
363 GFP foci was observed during meiosis. Rap1 motion in meiotic prophase I of the
364 *mps3-AAA* mutant is restricted to one area of NE (Figure 4C). Therefore, we
365 concluded that T188, S189, and S190 of Mps3 are important for meiotic telomere
366 dynamics. Indeed, the *mps3-AAA* mutant was defective in chromosome motion
367 as shown by analysis of a GFP fusion of Zip1 (Koszul *et al.* 2008). During
368 prophase I, Zip1-GFP shows dynamic motion (Figure 4D). The *mps3-AAA* mutant
369 reduced velocity of Zip1 motion by approximately 3-fold relative to the wild type
370 (48±15 versus 130±31 nm/sec, Figure 4E).
371 Next, we examined the localization of the Mps3-AAA mutant protein in
372 meiosis as a GFP fusion protein (Figures 4F). *mps3-AAA-GFP* cells showed 85%
373 of spore viability, which was comparable to the mutant stain without the GFP tag.

374 Similar to the wild-type Mps3-GFP, the Mps3-AAA GFP fusion protein normally
375 resided on the SPB as a single focus during mitosis (Figure 4F). During meiosis,
376 the Mps3-AAA mutant protein showed reduced NE localization. On entry into
377 meiosis, similar to the wild-type Mps3, the Mps3-AAA mutant protein formed a
378 few (usually two or three small) foci on NE, but showed little increase in the
379 number of Mps3 foci. At late time points, different from wild-type Mps3, the mutant
380 protein did not form an Mps3 patch or cover on NE (Figures 4F, 4G). Later, such
381 as at 6 h, two or three foci of Mps3 showed a limited movement (Figures 4H, 4I).
382 These results suggested that T188, S189, and S190 of Mps3 are necessary for
383 meiosis-specific Mps3 localization and motion on NE, particularly efficient
384 localization on NE accompanied with the formation of large complexes.
385 Interestingly, the Mps3-AAA-Flag mutant protein still bound to Ndj1 and Csm4
386 like wild-type Mps3 protein (Figure S3E), which is consistent with the Mps3-AAA
387 protein retains N-terminal nucleoplasmic region and SUN domain for Ndj1 and
388 Csm4 binding, respectively.
389
390 **The *mps3-AAA* mutant is deficient in NE growth**
391 In addition to localization/movement defects, the *mps3-AAA* mutant showed a
392 defect in nuclear morphology. First, the meiotic nucleus of the *mps3-AAA* mutant
393 was smaller than that of the wild type (Figure 4B). The nucleus of the wild type
394 grew when the cell underwent meiosis and exhibited a 4-fold increase (in area; 2
395 folds in length) at 4 h (Figure 4J). The treatment with LatB did not affect the
396 expansion, indicating that meiosis-specific NE remodeling does not require actin
397 polymerization. The *mps3-AAA* mutant showed defective NE growth in prophase
398 I; nuclear area in the *mps3-AAA* mutant is similar between 0 and 4 h (Figure 4M).
399 These indicate that Mps3 luminal region plays a critical role in the growth of the
400 meiotic nucleus, possibly by controlling NE remodeling.
401 Second, a fraction of the *mps3-AAA* mutant cells showed a partial defect in
402 telomere tethering to NE during meiosis. In one or two Rap1-GFP foci, the *mps3-*
403 *AAA* mutant (40%; n=100) was localized to the nucleoplasm rather than the
404 nuclear periphery, whereas all Rap1-GFP foci were localized near NE in the wild
405 type (Figure 4B). The weak telomere tethering defect in the *mps3-AAA* mutant is
406 reminiscent of the defect observed with an *NDJ1* mutant, which also showed a

407 partial tethering defect (Figure 4B) (Conrad et al., 1997; Trelles-Sticken et al.,
408 2000).
409
410 **Aspartate substitution of TSS in Mps3 suppress CDK and DDK defects**
411 We constructed a version of Mps3 with three negative charges on the TSS
412 sequence (T188D, S189D, and S190D), referred to as *MPS3-DDD* (Figure 3B).
413 The *MPS3-DDD* allele did not show any mitotic defects. The *MPS3-DDD* cells
414 showed wild-type spore viability and enter into MI like wild-type cells (Figure S3E,
415 F). The *MPS3-DDD* cells also displayed similar Rap1-GFP dynamics to wild-type
416 cells with normal clustering during prophase I (Figures 5A, 5B). The Mps3-DDD-
417 GFP protein localized to SPB during vegetative growth and showed wild-type like
418 localization on NE during meiosis (Figure 5C and Figure S3G). Mps3-DDD-GFP
419 displayed movement that was similar to that of the wild-type protein (Figures 5C).
420 The aspartate substitutions of Mps3 suppressed the resolution defect in Rap1
421 clustering at late time points of meiosis by CDK and DDK inactivation (Figures
422 5B, 5C), although some clustering persisted under the conditions (Figure 5B).
423 Mps3-DDD-GFP showed NE localization and movement during meiosis even
424 under the conditions of either CDK or DDK inactivation (Figures 5C, 5D), which
425 is similar to that in wild type Mps3-GFP and Mps3-DDD-GFP cells. Clustering of
426 Mps3 induced by CDK/DDK inactivation was clearly ameliorated by the
427 introduction of Mps3-DDD-GFP (Figures 5C,5C). However, there are some
428 restricted motion of Mps3-DDD protein under CDK/DDK inactivation relative to
429 Mps3-DDD protein, suggesting CDK/DDK activities are still required for wild-type
430 levels of Mps3 motion (Figure 5E), which may reflect partial rescue of resolution
431 defect in Rap1 clustering. Importantly, NE localization and dynamics of Mps3-
432 DDD protein still depends on meiosis. In vegetative cells, Mps3-DDD cells shows
433 SPB localization of Mps3-DDD and normal Rap1 localization (Figure S3H, S3I).
434 These results suggested that Mps3-DDD protein does not depend on CDK and
435 DDK for its meiosis-specific dynamics on NE.
436 Surprisingly, Mps3-DDD, not wild-type Mps3, show NE localization in mitotic
437 cells only in the *cdc7 bob-1* mutant, but not in the *cdc7as3* with the inhibitor
438 (Figure 5C). This suggests that, different from meiosis, DDK negatively regulates
439 NE localization of Mps3 in vegetative cells.

440

441 **Luminal region of Mps3 binds to membrane *in vitro***

442 To know the role of putative phosphorylation of Mps3 luminal region, we analyzed
443 biophysical properties of a 55 amino acid Mps3 peptide (153-208 aa) containing
444 both transmembrane (TM) and luminal regions (Figure 3A). The luminal region is
445 referred to as juxtamembrane (JM) region (Figure 6A). We prepared two peptides,
446 Mps3-wild type (WT) and Mps3-DDD, which contains three aspartates (Figure
447 6A). Synthesized Mps3 peptides were mixed with liposome comprised of
448 POPC/POPS (10/3)(Sato et al., 2006) First, we checked conformation of each
449 peptides in the bilayers by polarized FT-IR (Fourier-transform Infrared
450 spectroscopy) and found both Mps3-WT and Mps3-DDD peptides contained
451 similar content of α-helix and β-strand (Figure S4A). Dichroic ratio calculated for
452 Mps3-WT and Mps3-DDD were 2.90 and 2.85, suggesting that both
453 transmembrane regions are inserted into lipid bilayers with a similar tilt angle of
454 ~30° relative to the membrane normal (Tamagaki et al., 2014). We cannot assign
455 those peaks from β-strand to which residues in the JM regions are involved for
456 the β-structure with this FT-IR experiment alone.

457 We next synthesized Mps3 TM-JM peptide with Alexa fluorophore-dye
458 (Alexa-568) at the C-terminus of the JM region and analyzed spectrum of the dye
459 in presence of different concentrations of negatively charged PIP_2 (phosphatidyl-
460 inositol 4,5-bisphosphate), which modulates status of charge on the membrane
461 surface (Sato et al., 2009b). Here we utilized PIP_2-involving model system to see
462 if the JM gets affected by membrane although we are aware of the fact that it has
463 not been known whether Msp3 interacts with PIP_2. This simple model system
464 must provide a possible mechanism of how negative charge on the JM region
465 caused by its phosphorylation affect its behavior against the membrane.

466 For the wild-type peptide, the addition of PIP_2 decreased the peak intensity
467 of fluorophore at 600 nm up to ~40% (Figure 6B). The triplicate showed similar
468 results. Decreased fluorescence could be due to quenching of the fluorescence
469 from the dye association (self-quenching) by inter-peptide association (Figure
470 6C) as shown in the previous study on an ErbB2 peptide containing TM and JM
471 regions (Matsushita et al., 2013). These results suggest that the JM region of the
472 Mps3-WT peptide is sensitive to the change in the membrane component and

473 also that the JM regions interact with the acidic lipid bilayer. On the other hand,
474 Mps3-DDD peptide decreased the intensity to ~20% (a half of the intensity from
475 WT peptide). The decrease in the change in the fluorescence intensity must be
476 due to two types of electrostatic repulsion, between side chains of the aspartates
477 on each JM regions and/or between the aspartates and the acidic lipids (Figure
478 6C). These repulsions must place the fluorophores apart preventing from self-
479 quenching. The latter repulsion can reduce the JM region of Mps3-DDD peptide
480 binding to the bilayers compared from that of the Mps3-WT. These suggest the
481 different conformation of Mps3-WT and -DDD peptides in respect of the
482 interaction of JM region of Mps3 to the membrane.

483 To get more insight on behavior of the JM region with the membrane, we
484 utilized a technique of molecular dynamic (MD) simulation. Since there is no
485 reported structure on the TM-JM region of Mps3, we artificially constructed the
486 initial structure of the TM-JM sequence as follow: using a software *Chimera*
487 (Pettersen et al., 2004), R161-M181 is set to be α-helix as the TM region; the rest
488 was set to be random structure. This constructed structure was embedded in
489 membrane (POPC/POPS/PIP_2=8:2:1 with 80 nm in XY dimension) using
490 *Membrane Builder* module in *CHARMM-GUI* (Jo et al., 2008). The peptide-
491 membrane system was fully hydrated in 150 mM NaCl solution.

492 Firstly, we performed coarse-grained molecular dynamics simulations on the
493 constructed TM-JM peptide in membrane. We ran simulations on two sequences,
494 Mps3-WT and Mps3-DDD. Duration of each run was >3 μs and three sets were
495 performed for each sequence. Results from all of the calculations showed that
496 the JM region from Mps3-DDD dissociated from the membrane (Figure S4B).
497 Conversely, that of Mps3-WT kept attached on the membrane (Figure S4B).
498 Secondly, we performed all-atom simulation on three TM-JM sequence peptides,
499 Mps3-WT, Mps3-DDD and Mps3-WT phosphorylated at T197-S198-S199.
500 Duration of each calculation was >50 ns. In Figure 6D, snap-shots from
501 trajectories for three sequences are shown. Results from the simulation, together
502 with mass density profiles (Figure S4C), indicate that JM regions from Mps3-DDD
503 and phosphorylated Mps3 dissociated from the membrane. On the other hand,
504 the JM region from Mps3-WT kept attached on the membrane.
505
506

507 **Discussion**

508 Here we described the multilayered control of the dynamics of a NE protein with
509 SUN domain, Mps3, during yeast meiosis. In both mitotic and meiotic cells, Mps3
510 is a major component of a half bridge as well as SPIN (SPB interacting network)
511 (Chen et al., 2019; Lee et al., 2020) (Li et al., 2017). Meiosis induces the
512 localization and motion of Mps3 on NE, which are accompanied with the
513 formation of a large protein ensembles in NE as the LINC complex detected as
514 foci/patches. The meiosis-specific LINC complex tethers telomeres and interacts
515 with cytoplasmic actin cables. In a luminal region between INM and ONM, Mps3
516 binds to a KASH protein, Mps2, both during mitosis and meiosis, and to a
517 meiosis-specific Mps2-binding protein, Csm4 (Chen et al., 2019; Lee et al., 2020).
518 Mps2 and Csm4 cooperate for the binding to the motor Myo2 in cytoplasm. Myo2
519 on actin cables, which is induced in meiotic cells, generates forces for the motion
520 of the LINC complex on NE, which in turn move chromosomes inside of meiotic
521 cells (rapid prophase movement; RPM) as well as the clustering of telomeres in
522 zygotene stage (Conrad et al., 2008; Koszul et al., 2008; Trelles-Sticken et al.,
523 2000; Trelles-Sticken et al., 1999). While Mps3 localization on NE is independent
524 of actin-generated force (and other meiosis specific factors such as Ndj1 and
525 Csm4), Mps3 movement on NE is dependent of the force. Meiosis-specific Mps3
526 modulation promotes the formation of a LINC complex containing Mps3 for
527 meiotic events such as chromosome pairing/synapsis, and chromosome motion
528 as well as NE expansion.

529 Localization of Mps3 on NE in meiotic cells is divided into several distinct
530 steps (Figures 1A and 7); 1) In addition to the SPB, at early times in prophase I,
531 a few Mps3 foci appear on NE. 2) With increased numbers of the foci, patches of
532 Mps3, large cohesive ensembles with multiple foci, are formed on NE, which
533 sometimes associated with clustering in one area of NE. 3) Multiple foci and
534 patches cover on entire NE. 4) Mps3 shows continuous coverage on NE
535 (sometimes with a hole at nucleus-vacuole junction; NVJ). 5) During late
536 prophase I or pro-metaphase I, most of Mps3 on NE disappear from NE, leaving
537 two SPB-associating foci. At each stage, Mps3 foci/patches show RPM which is
538 maximum at mid/late prophase I (Conrad et al., 2008; Koszul et al., 2008; Trelles-
539 Sticken et al., 2000; Trelles-Sticken et al., 1999).

540 In this study, we found that two cell-cycle kinases, CDK and DDK, promote
541 proper Mps3 localization on NE during meiosis, particularly the resolution of
542 clustered Mps3 foci (and, thus, telomere clustering), suggesting that the
543 phosphorylation of a target protein(s) plays a role in resolution of Mps3 clusters.
544 Moreover, we showed that the JM region of Mps3 near INM, which is located in
545 lumen of NE, is critical for the NE localization of the protein. S179 and S180, and,
546 probably T178, of the JM region seems to be subject to meiosis-specific
547 phosphorylation. We also showed that introducing negative charges in the JM
548 region changes the binding ability of the region to the membrane in reconstituted
549 liposomes. These support the idea that Mps3 localization on NE is a part of a
550 novel meiotic regulatory system known as "NE remodeling." Probably, non-
551 canonical phosphorylation of the JM region is likely to promote the meiosis-
552 specific NE localization of Mps3.
553
554 **Phosphorylation of NE luminal region**
555 Although our results described here suggest one intriguing hypothesis that CDK
556 and DDK collaborate to catalyze the phosphorylation of the JM region of Mps3
557 for its NE localization, this is less likely for several reasons. It is unlikely that CDK
558 and DDK are responsible for direct phosphorylation reaction in lumen
559 compartments. These kinases are not localized to luminal regions of both
560 endoplasmic reticulum (ER) and NE since the catalytic subunits (Cdc28 and
561 Cdc7) and its regulatory subunits (Clb5,6 and Dbf4) lack a leader sequence
562 necessary for the luminal localization.
563 The protein phosphorylation of the luminal region between INM and ONM
564 is very unusual, and have not been reported in the past. On the other hand, recent
565 studies have shown that the phosphorylation of secreted proteins and
566 oligosaccharides of membrane proteins is catalyzed by an atypical kinase such
567 as Fam20C in the lumen of Golgi apparatus and ER in vertebrate cells
568 (Tagliabracci et al., 2012; Tagliabracci et al., 2013; Tagliabracci et al., 2015).
569 Fam20C, whose structure and sequence are divergent from typical kinases, uses
570 ATP as a donor of phosphate, but prefers Mn^{2+} rather than Mg^{2+} for the catalysis
571 (Tagliabracci et al., 2012; Tagliabracci et al., 2013; Tagliabracci et al., 2015).
572 Given a luminal region of NE is continuous to that of ER where INM/ONM proteins

are synthesized, it is possible that a similar activity to Fam20C family might be present in the lumen between INM and ONM, which may catalyze the phosphorylation of NE luminal region of Mps3. However, there is no report on the presence of Fam20C orthologues or relative enzymes in lower eukaryotes such as yeasts. Alternatively, the phosphorylation of the luminal region might be mediated by a novel mechanism. Given membranes are rich in phospho-lipids, the phosphate group in the lipids as a donor might be transferred to proteins by a novel mechanism. We need further studies to identify a protein responsible for the phosphorylation of JM region of Mps3.

A previous study showed that S70 in the nucleoplasmic region of Mps3 is phosphorylated during late prophase I, which facilitates the removal of the N-terminal region of Mps3 by proteosome-dependent cleavage (Li et al., 2017). This removal may play a role in disappearance of Mps3 from NE in late prophase I and for separation of duplicated SPBs (Li et al., 2017). During meiosis of *C. elegans*, the N-terminal nucleoplasmic region of Sun-1 protein is phosphorylated by Chk-1 and Cdk-1 (Penkner et al., 2009; Zuela and Gruenbaum, 2016). In M phase of human cells, SUN1 protein is phosphorylated at its N-terminal region by CDK and PLK (Patel et al., 2014). Together with results described here, these suggest the importance of the phosphorylation in the regulation of dynamics and/or regulation of SUN-domain proteins.

Th role of negative charges in JM region of Mps3

Biophysical analysis of synthetic peptides containing TM and JM regions of Mps3 in synthetic liposomes revealed that the JM region of Mps3 has a capability to bind to the lipid bilayers. Importantly, introducing three negative charges in the JM region weakens the binding to the membrane, resulting in a change of geometry of JM region of Mps3, as extension, the luminal region of Mps3 including SUN domain. As a typical LINC complex, SUN domain of Mps3 in INM binds to KASH domain of Msp2 in ONM. The connection would span ~20 nm between INM and ONM (Chen et al., 2019; Lee et al., 2020). Recently, Jasperson and her colleagues showed “atypical” configuration of Mps3-Mps2, in which not only SUN-KASH interaction, but also N-terminal regions of both Mps3 and Mps2 bind to each other in SPIN which surrounds SPB (Chen et al., 2019; Lee et al.,

606 2020). Typical LINC could accommodate *trans*-membrane configuration in the
607 luminal region while atypical LINC would do *cis*-membrane configuration (Figure
608 7). These suggest that luminal regions of Mps3 and Mps2 are quite flexible to
609 accommodate two different SUN-KASH configurations. Our results support that
610 the switch from *cis*- to *trans*-membrane configurations might be regulated by the
611 binding of the JM region of Mps3 to the INM. While the interaction between JM
612 region of Mps3 and INM promotes *cis*-membrane form of noncanonical LINC
613 complex, negative charges induced by phosphorylation may reduce the
614 interaction between JM and INM, which in turn might accommodate a
615 conformation suitable for the *trans*-membrane form. Alternatively, negatively
616 charged JM region of Mps3 would be a binding site of the other protein which
617 may promote the configuration switch.
618
619 **What is a target by CDK- and DDK in chromosome motion?**
620 In this study, we showed that, in the budding yeast, two cell cycle kinases, CDK
621 and DDK, collaborate in meiotic telomere dynamics by regulating proper
622 localization of Mps3 on NE. As discussed above, it is unlikely that CDK and DDK
623 directly phosphorylate the luminal region of Mps3. Moreover, the comparison of
624 *cdk/ddk* mutants with the *mps3-AAA* mutant reveals the difference in meiotic
625 defects in Mps3 localization. CDK/DDK inactivation results in persistent telomere
626 clustering with Mps3 polarized localization. These indicate that CDK and DDK
627 activities promote the resolution of Mps3 foci/patches and/or telomeres rather
628 than the NE localization *per se*. Mps3 localization on NE seems be normal even
629 in the absence of CDK and DDK activities. Phenotypic similarity between *cdk* and
630 *ddk* mutants on Mps3 localization suggests a common target of these kinases for
631 the resolution of the clusters. It is well known that CDK phosphorylation primes
632 the DDK phosphorylation, which is seen in Mer2 phosphorylation during meiosis
633 (Henderson et al., 2006; Sasanuma et al., 2008; Wan et al., 2008). Interestingly,
634 telomere-resolution defects under CDK and DDK inactivation are similar to that
635 in the mutant of the *REC8* gene (Challa et al., 2016), which encodes a meiosis-
636 specific kleisin subunit of the cohesin complex (Klein et al., 1999) and cohesin
637 regulator, *RAD61/WPL1* (Challa et al., 2016). It is well known that Rec8 is
638 phosphorylated by DDK (and Polo and CK1 kinases), but not by CDK (Katis et

al., 2010) and that Rad61/Wpl1 is phosphorylated by DDK and Polo-like kinase (PLK). Thus, there might be the other target in cohesin components by these kinases. In mitotic yeast cells, Eco1, which catalyzes acetylation of Smc3 cohesin subunit, is phosphorylated by CDK and DDK for the degradation (Seoane and Morgan, 2017). Interestingly, Eco1 is shown to acetylate Mps3 in vegetative cells (Ghosh et al., 2012).

Telomere clustering during prophase I persists with CDK or DDK inactivation, suggesting the presence of a constraint on the resolution of the clustering. The phosphorylation, thus negative charges, in JM region, might overcome the constraint for the resolution. This is supported by the fact that the *MPS3-DDD* partially rescued the resolution defect of telomere clustering with CDK or DDK inactivation. Moreover, we found Mps3-DDD, not wild-type Mps3, show NE localization in mitotic cells only in the *cdc7 bob-1* mutant (Figure 5C), suggesting the presence of DDK-dependent constraints on NE localization of Mps3 during mitosis.

Meiosis establishes Mps3 localization on NE

As described above, Mps3 localization on NE is regulated in distinct stages (Figure 7). The *mps3-AAA* mutant still retains an ability to form early meiosis-specific Mps3 foci on NE. And also Mps3-DDD protein needs meiosis for NE localization during meiosis. These suggest that Mps3 localization on NE is initiated and/or established during early meiotic prophase I. Given that Mps3 localization as an ensemble on NE is specific to meiosis, there might be an early meiosis-specific factor or modification that regulates the establishment of the Mps3 localization as an ensemble on NE upon the entry into meiosis. We examined two meiosis-specific factors, Ndj1 and Csm4, both of which are involved in chromosome motion and Mps3 dynamics, but it is unlikely that these factors function in the establishment of Mps3 localization. Further work is necessary to identify the factors necessary for the initiation event of NE remodeling.

We showed that non-canonical phosphorylation of the luminal JM region of Mps3 promotes the formation of multiple Mps3 foci/patches on NE. The *mps3-AAA* mutant is deficient in the transition to early Mps3 foci to middle Mps3

foci/patches, suggesting the role of negative charges in JM region in the transition, thus the maintenance of Mps3 localization on NE.

NE remodeling controls various nuclear events

Characterization of the *mps3-AAA* single mutant revealed that Mps3 localization to NE (NE remodeling) play multiple roles during meiosis. As expected from previous reports (Koszul et al., 2008; Scherthan et al., 2007), Mps3-dependent NE remodeling is important for chromosome motion and thus chromosome pairing/synapsis. Mps3 phosphorylation seems to be essential for the formation of active NE-bound ensembles for chromosome motion via recruitment of various proteins and promotion of telomere tethering. Moreover, we found that the *mps3-AAA* single mutant is defective in meiosis-specific enlargement of nuclei, which presumably is facilitated by NE expansion. NE-bound Mps3 may regulate NE growth by directly promoting lipid synthesis on NE or importing lipids from the ER (Sosa Ponce et al., 2020).

Materials and Methods

Strains and plasmids

All strains described here are derivatives of SK1 diploids and are described in Table S1. Strain construction is described in the Extended Experimental Procedures. GST fusion genes of a PCR-amplified Mps3 fragment (160–260 amino acid residues of the Mps3 protein) were constructed on pGEX-2T.

Anti-serum and antibodies

Anti-HA antibody (16B12; Babco), anti-Flag (M2, Sigma), anti-tubulin (MCA77G, Bio-Rad/Serotec, Ltd), anti-GFP (3E6; Molecular Probes), and rabbit anti-Dmc1 (Shinohara et al., 2000) were used for staining. Anti-Zip1 (rabbit) and anti-Red1 (chicken) were described previously (Shinohara et al., 2008). Rabbit anti-Rec8 antibody was described previously (Rao et al., 2011). Guiana pig anti-Hop1 serum was described in (Bani Ismail et al., 2014). The second antibodies for staining were Alexa-488 (Goat) and -594 (Goat) IgG used at a 1/2000 dilution (Themo Fishers).

10 amino acid of Mps3 peptide with 189-phosphoserine and 190-phosphoserine (186-GAT**pSpS**PGKSF-195) was synthesized and used for the immunization of rabbit. From obtained serum, antibody specific phosphor-peptide was affinity-purified using the phosphor-peptide (MBL Co. Ltd. Japan).

Cytology

Time-lapse images of Mps3-GFP, Rap1-GFP and Zip1-GFP were captured using a computer-assisted fluorescence microscope system (DeltaVision; Applied Precision). The objective lens was an oil immersion lens (100×; NA, 1.35). Image deconvolution was performed using an image workstation (SoftWorks; Applied Precision). Time-lapse image acquisition was performed every 0.5 to 1 s at a single focal plane. Meiotic cell cultures (~150μl) were placed on bottom-glass dishes (Matsunami) pre-coated with Concavalin A (10 mg/ml, Sigma)

The sectioned area of each nucleus with Rap1-GFP, which showed nuclear and dotty staining, was measured using the Velocity™ program (Applied Precision) with manual assignment of the rim of the sectioned area. Ninety-six

722 nuclei were counted. Tracking of Zip1-GFP/Mps3-GFP/Rap1-GFP was analyzed
723 using the ImageJ program (NIH) and plug-in MTrack2 (Nico Shuuman).
724
725 **IP and Western blotting**
726 Yeast cell lysates were prepared by the glass bead disruption method. The
727 lysates were incubated with magnetic beads (Dynal M260; GE Healthcare)
728 coated with anti-Flag antibody (M2, Sigma) for 12 h and washed extensively.
729 Bound proteins were eluted by adding the SDS sample buffer and were analyzed
730 on an SDS-PAGE gel, transferred to a nylon membrane (Millipore Co. Ltd), and
731 probed with specific antibodies.
732
733 **Analyses of meiotic recombination**
734 Time-course analyses of DNA events in meiosis and cell cycle progression were
735 performed as described previously (Shinohara et al., 1997; Storlazzi et al., 1996).
736
737 **Southern Blotting**
738 Southern blotting analysis was performed with the same procedure as in
739 (Storlazzi et al., 1995). For the *HIS4-LEU2* locus, genomic DNA prepared was
740 digested with *Xho*I (for crossover) and *Pst*I (for meiotic DSBs). For the *URA3-*
741 *ARG4* locus, the DNA were digested with *Xho*I. Probes for southern blotting were
742 Probe 155 for crossover and Probe 291 for DSB detection on the *HIS4-LEU2* as
743 described in (Xu et al., 1995). Image gauge software (Fujifilm Co. Ltd., Japan)
744 was used for quantification for bands.
745
746 ***In vitro* kinase assay**
747 For *in vitro* phosphorylation, 1 μg of purified GST-Mps3 or GST-Mps3-AAA was
748 incubated with γ-^{32}P-ATP (100 μM; 2.2 MBq) in the presence of CDK (~0.2μg)
749 and/or DDK (~0.2μg) in a 20 μl of buffer [20 mM Tris-HCl (pH 7.5), 10 mM $MgCl_2$,
750 10 mM β-glycerophosphate]. After 1-h incubation at 30°C, the reaction was
751 stopped by adding 5× SDS-PAGE sample buffer, and the products were analyzed
752 on 10% SDS-PAGE gel. Dried gels were analyzed using a phosphorimager BAS
753 2000 (Fuji Co. Ltd).
754

755 **Synthesis of Mps3 peptides**

756 Peptides with the TM and JM region of Mps3 (residue 153-208) were synthesized
757 by solid-phase method with the following sequence:
758 GEAKKLKWRTYIFYGGLFFVFYFFGSFLMTTVKNNDLESHSSGA**TSS**PGKSFS
759 NL-Cys and
760 GEAKKLKWRTYIFYGGLFFVFYFFGSFLMTTVKNNDLESHSSGA**DDD**PGKSF
761 SNL-Cys (underlines indicate TM region). The synthetic peptides were purified
762 by reverse-phase HPLC on a C4 column with gradient of 2-propanol over water
763 containing 0.1% trifluoroacetic acid. For fluorescent-labeling, Alexa Fluor 568 C5-
764 maleimide (Molecular probe) was introduced to the sulfide group on cysteine by
765 mixing the peptides and the fluorescent dye in dimethylformamide under basic
766 conditions.

767

768 **Preparation of lipid bilayer with peptides**

769 The Mps3 peptides were co-solubilized with 1-palmitoyl-2-oleoyl-*sn*-
770 phosphatidycholine (POPC), 1-palmitoyl-2-oleoyl-*sn*-phosphatidyserine (POPS)
771 and octyl-β-glucoside in trifluoroethanol (TFE). The peptide to lipid molar ratio
772 was 1:100. The lipid concentration was 200 μM. The ratio of POPC and POPS
773 was 10:3. The mixture was incubated for 90 min at 37°C. Then TFE was
774 removed under stream of Ar. MES buffer (10 mM MES, 50 mM NaCl, and 5 mM
775 DTT, pH 6.2) was added to the solid from the previous step and mixed at 37 °C
776 for 6 h. The octyl- β -glucoside was removed by dialysis against the MES buffer.

777

778 **Measurement of FT-IR**

779 Polarized attenuated total reflection FT-IR spectra were obtained on a JASCO
780 FT/IR-4700 spectrometer. Membranes containing Mps3 TM–JM peptides were
781 layered on a germanium internal reflection element using a slow flow of nitrogen
782 gas directed at an oblique angle to the IR plate to form an oriented multilamellar
783 lipid–peptide film.1000 scans were acquired and averaged for each sample at a
784 resolution of 4 cm^{-1}. The absorption of polarized light by the amide I bond yields
785 the dichroic ratio defined as a ratio of absorption intensity for parallel, relative to
786 perpendicular, polarized light. From the dichroic ratio, we estimated the tilt angle
787 of the TM helix relative to the membrane normal based on the method described

by Smith and coworkers (Liu et al., 2004; Smith et al., 2002)) using a value of 41.8° for angle α between the helix director and the transition-dipole moment of the amide I vibrational mode. For the FT-IR experiment, the amount of lipid used per experiment was ~4 mg. The film on the ATR plate in our experiment was assumed to be greater than ~10 μm. For calculating the dichroic ratio, the thick film limit is applicable (Bechinger et al., 1999). Equations that we used for the calculation of the dichroic ratios were based on this assumption.

Fluorescence spectroscopy

For experiments with PIP_2, TM-JM peptides were inserted into POPC/POPS membrane as explained above. The peptide/lipid ratio was set to 1:1000 for observing the fluorescence from Alexa568. The lipid concentration was 200–250 μM in MOPS buffer (1 mM MOPS, 0.1 M KCl, pH 7.0). Vesicles were formed by extrusion of multilamellar vesicles through 200-nm polycarbonate filters. PIP_2 were added into the membranes by addition of PIP_2 micelles to the vesicle solution. Fluorescence was measured within 1 hour to minimize PIP_2 hydrolysis. The PIP_2 concentration was from 5 μM to 25 μM. Fluorescence measurement was carried out on HITACHI F-2500 fluorescence spectrophotometer at the excitation wavelength of 568 nm.

Coarse-grained MD simulation

All simulations were performed using GROMACS 2016 package (Abraham et al., 2015) using the MARTINI force field with polarizable water (Marrink et al., 2007). Periodic boundary conditions were applied in all directions, and the time step was 20 fs. The temperature was controlled with the Berendsen temperature coupling scheme (Berendsen et al., 1984)with a time constant of 1 ps, and the pressure was controlled using the Parrinello–Rahman semi-isotropic barostat (Parrinello and Rahman, 1981) with a time constant of 12 ps and a compressibility of 3×10^{-4} bar $^{-1}$. All the simulations were carried out in the isothermal–isobaric (NPT) ensemble at a temperature of 303 K and pressure of 1.0 bar. The cut-off of the Van der waals interactions were set to 1.1 nm.

All atom MD simulation

The NAMD software package (Phillips et al., 2005) was used to perform all-atom MD simulations. The CHARMM36m force field (Huang et al., 2017) together with TIP3P water model were used for all simulations. All simulations in NPT dynamics (constant particle number, pressure and temperature) were carried out at 303 K with Langevin dynamics, and at 1 atm maintained by Nosè-Hoover Langevin piston method. Full electrostatic interactions were treated by the particle mesh Ewald (PME) approach with a grid spacing of less than 1 Å. The cut-off radii of long-range electrostatic and van der Waals interactions were set to be 12 Å, with a smoothing function applied from 10 Å.

Acknowledgments

We are grateful to Drs. Nancy Hollingsworth, Franz Klein, Kunihiro Ohta, Kazu Nishikawa, Hisao Masai, and Hiroyuki Araki for providing the materials used in this study. HBDPR was supported by the BMC program and a scholarship from the Graduate School of Science, Osaka University, JASSO as well as MEXT. KC KC were supported by the Institute for Protein Research. This work was supported by a Grant-in-Aid from the JSPS KAKENHI Grant Number; 22125001, 22125002, 15H05973 and 16H04742, 19H00981 to A.S.

Competing interest

The authors declare no competing financial interest.

Author contributions

H.B.D.P.R., T.S., K.C., M.S. and A.S. designed the experiments. H.B.D.P.R., T.S., K.C., M.S. and A.S. carried out experiments. M.S provided materials. H.B.D.P.R., T.S., K.C. and A.S. analyzed the data. A.S. wrote the manuscript with inputs from H.B.D.P.R., T.S., K.C. and M.S.

References

Abraham, M.J., T. Murtola, R. Schulz, S. Páll, J.C. Smith, B. Hess, and E. Lindahl. 2015. GROMACS: High performance molecular simulations through multi-level parallelism from laptops to supercomputers. *SoftwareX*. 1-2:19-25.

Bani Ismail, M., M. Shinohara, and A. Shinohara. 2014. Dot1-dependent histone H3K79 methylation promotes the formation of meiotic double-strand breaks in the absence of histone H3K4 methylation in budding yeast. *PloS one*. 9:e96648.

Bechinger, B., J.M. Ruysschaert, and E. Goormaghtigh. 1999. Membrane helix orientation from linear dichroism of infrared attenuated total reflection spectra. *Biophysical journal*. 76:552-563.

Benjamin, K.R., C. Zhang, K.M. Shokat, and I. Herskowitz. 2003. Control of landmark events in meiosis by the CDK Cdc28 and the meiosis-specific kinase Ime2. *Genes & development*. 17:1524-1539.

Berendsen, H.J.C., J.P.M. Postma, W.F.v. Gunsteren, A. DiNola, and J.R. Haak. 1984. Molecular dynamics with coupling to an external bath. *The Journal of Chemical Physics*. 81:3684-3690.

Challa, K., M.S. Lee, M. Shinohara, K.P. Kim, and A. Shinohara. 2016. Rad61/Wpl1 (Wapl), a cohesin regulator, controls chromosome compaction during meiosis. *Nucleic Acids Res*. 44:3190-3203.

Chen, J., J.M. Gardner, Z. Yu, S.E. Smith, S. McKinney, B.D. Slaughter, J.R. Unruh, and S.L. Jaspersen. 2019. Yeast centrosome components form a noncanonical LINC complex at the nuclear envelope insertion site. *J Cell Biol*. 218:1478-1490.

Chikashige, Y., T. Haraguchi, and Y. Hiraoka. 2007. Another way to move chromosomes. *Chromosoma*. 116:497-505.

Chua, P.R., and G.S. Roeder. 1997. Tam1, a telomere-associated meiotic protein, functions in chromosome synapsis and crossover interference. *Genes & development*. 11:1786-1800.

Conrad, M.N., A.M. Dominguez, and M.E. Dresser. 1997. Ndj1p, a meiotic telomere protein required for normal chromosome synapsis and segregation in yeast. *Science (New York, N.Y.)*. 276:1252-1255.

Conrad, M.N., C.Y. Lee, G. Chao, M. Shinohara, H. Kosaka, A. Shinohara, J.A.

Conchello, and M.E. Dresser. 2008. Rapid telomere movement in meiotic prophase is promoted by NDJ1, MPS3, and CSM4 and is modulated by recombination. *Cell*. 133:1175-1187.

Conrad, M.N., C.Y. Lee, J.L. Wilkerson, and M.E. Dresser. 2007. MPS3 mediates meiotic bouquet formation in Saccharomyces cerevisiae. *Proc Natl Acad Sci U S A*. 104:8863-8868.

Cool, M., and R.E. Malone. 1992. Molecular and genetic analysis of the yeast early meiotic recombination genes REC102 and REC107/MER2. *Molecular and cellular biology*. 12:1248-1256.

Engebrecht, J., J. Hirsch, and G.S. Roeder. 1990. Meiotic gene conversion and crossing over: their relationship to each other and to chromosome synapsis and segregation. *Cell*. 62:927-937.

Ghosh, S., J.M. Gardner, C.J. Smoyer, J.M. Friederichs, J.R. Unruh, B.D. Slaughter, R. Alexander, R.D. Chisholm, K.K. Lee, J.L. Workman, and S.L. Jaspersen. 2012. Acetylation of the SUN protein Mps3 by Eco1 regulates its function in nuclear organization. *Mol Biol Cell*. 23:2546-2559.

Hawley, R.S., and W.D. Gilliland. 2009. Homologue pairing: getting it right. *Nature cell biology*. 11:917-918.

Henderson, K.A., K. Kee, S. Maleki, P.A. Santini, and S. Keeney. 2006. Cyclin-dependent kinase directly regulates initiation of meiotic recombination. *Cell*. 125:1321-1332.

Hiraoka, Y., and A.F. Dernburg. 2009. The SUN rises on meiotic chromosome dynamics. *Dev Cell*. 17:598-605.

Huang, J., S. Rauscher, G. Nawrocki, T. Ran, M. Feig, B.L. de Groot, H. Grubmüller, and A.D. MacKerell, Jr. 2017. CHARMM36m: an improved force field for folded and intrinsically disordered proteins. *Nature methods*. 14:71-73.

Jackson, A.L., P.M. Pahl, K. Harrison, J. Rosamond, and R.A. Sclafani. 1993. Cell cycle regulation of the yeast Cdc7 protein kinase by association with the Dbf4 protein. *Molecular and cellular biology*. 13:2899-2908.

Jaspersen, S.L., T.H. Giddings, Jr., and M. Winey. 2002. Mps3p is a novel component of the yeast spindle pole body that interacts with the yeast centrin homologue Cdc31p. *J Cell Biol*. 159:945-956.

Jo, S., T. Kim, V.G. Iyer, and W. Im. 2008. CHARMM-GUI: A web-based graphical user interface for CHARMM. *Journal of Computational Chemistry*. 29:1859-1865.

Katis, V.L., J.J. Lipp, R. Imre, A. Bogdanova, E. Okaz, B. Habermann, K. Mechtler, K. Nasmyth, and W. Zachariae. 2010. Rec8 phosphorylation by casein kinase 1 and Cdc7-Dbf4 kinase regulates cohesin cleavage by separase during meiosis. *Dev Cell*. 18:397-409.

Klein, F., P. Mahr, M. Galova, S.B. Buonomo, C. Michaelis, K. Nairz, and K. Nasmyth. 1999. A central role for cohesins in sister chromatid cohesion, formation of axial elements, and recombination during yeast meiosis. *Cell*. 98:91-103.

Kosaka, H., M. Shinohara, and A. Shinohara. 2008. Csm4-dependent telomere movement on nuclear envelope promotes meiotic recombination. *PLoS genetics*. 4:e1000196.

Koszul, R., K.P. Kim, M. Prentiss, N. Kleckner, and S. Kameoka. 2008. Meiotic chromosomes move by linkage to dynamic actin cables with transduction of force through the nuclear envelope. *Cell*. 133:1188-1201.

Koszul, R., and N. Kleckner. 2009. Dynamic chromosome movements during meiosis: a way to eliminate unwanted connections? *Trends in cell biology*. 19:716-724.

Lee, C.Y., C.G. Bisig, M.M. Conrad, Y. Ditamo, L. Previato de Almeida, M.E. Dresser, and R.J. Pezza. 2020. Extranuclear Structural Components that Mediate Dynamic Chromosome Movements in Yeast Meiosis. *Current biology : CB*. 30:1207-1216.e1204.

Li, P., H. Jin, B.A. Koch, R.L. Abblett, X. Han, J.R. Yates, 3rd, and H.G. Yu. 2017. Cleavage of the SUN-domain protein Mps3 at its N-terminus regulates centrosome disjunction in budding yeast meiosis. *PLoS genetics*. 13:e1006830.

Liu, W., M. Eilers, A.B. Patel, and S.O. Smith. 2004. Helix packing moments reveal diversity and conservation in membrane protein structure. *Journal of molecular biology*. 337:713-729.

Marrink, S.J., H.J. Risselada, S. Yefimov, D.P. Tieleman, and A.H. de Vries. 2007. The MARTINI Force Field: Coarse Grained Model for Biomolecular

Simulations. *The Journal of Physical Chemistry B*. 111:7812-7824.

Matsushita, C., H. Tamagaki, Y. Miyazawa, S. Aimoto, S.O. Smith, and T. Sato. 2013. Transmembrane helix orientation influences membrane binding of the intracellular juxtamembrane domain in Neu receptor peptides. *Proc Natl Acad Sci U S A*. 110:1646-1651.

Nishikawa, S., Y. Terazawa, T. Nakayama, A. Hirata, T. Makio, and T. Endo. 2003. Nep98p is a component of the yeast spindle pole body and essential for nuclear division and fusion. *J Biol Chem*. 278:9938-9943.

Parrinello, M., and A. Rahman. 1981. Polymorphic transitions in single crystals: A new molecular dynamics method. *Journal of Applied Physics*. 52:7182-7190.

Patel, J.T., A. Bottrill, S.L. Prosser, S. Jayaraman, K. Straatman, A.M. Fry, and S. Shackleton. 2014. Mitotic phosphorylation of SUN1 loosens its connection with the nuclear lamina while the LINC complex remains intact. *Nucleus (Austin, Tex.)*. 5:462-473.

Penkner, A.M., A. Fridkin, J. Gloggnitzer, A. Baudrimont, T. Machacek, A. Woglar, E. Csaszar, P. Pasierbek, G. Ammerer, Y. Gruenbaum, and V. Jantsch. 2009. Meiotic chromosome homology search involves modifications of the nuclear envelope protein Matefin/SUN-1. *Cell*. 139:920-933.

Pettersen, E.F., T.D. Goddard, C.C. Huang, G.S. Couch, D.M. Greenblatt, E.C. Meng, and T.E. Ferrin. 2004. UCSF Chimera—A visualization system for exploratory research and analysis. *Journal of Computational Chemistry*. 25:1605-1612.

Phillips, J.C., R. Braun, W. Wang, J. Gumbart, E. Tajkhorshid, E. Villa, C. Chipot, R.D. Skeel, L. Kalé, and K. Schulten. 2005. Scalable molecular dynamics with NAMD. *J Comput Chem*. 26:1781-1802.

Rao, H.B., M. Shinohara, and A. Shinohara. 2011. Mps3 SUN domain is important for chromosome motion and juxtaposition of homologous chromosomes during meiosis. *Genes Cells*. 16:1081-1096.

Sasanuma, H., K. Hirota, T. Fukuda, N. Kakusho, K. Kugou, Y. Kawasaki, T. Shibata, H. Masai, and K. Ohta. 2008. Cdc7-dependent phosphorylation of Mer2 facilitates initiation of yeast meiotic recombination. *Genes & development*. 22:398-410.

984 Sato, A., B. Isaac, C.M. Phillips, R. Rillo, P.M. Carlton, D.J. Wynne, R.A. Kasad,
985 and A.F. Dernburg. 2009a. Cytoskeletal forces span the nuclear envelope
986 to coordinate meiotic chromosome pairing and synapsis. *Cell*. 139:907-
987 919.
988 Sato, T., P. Pallavi, U. Golebiewska, S. McLaughlin, and S.O. Smith. 2006.
989 Structure of the membrane reconstituted transmembrane-juxtamembrane
990 peptide EGFR(622-660) and its interaction with Ca2+/calmodulin.
991 *Biochemistry*. 45:12704-12714.
992 Sato, T., T.C. Tang, G. Reubins, J.Z. Fei, T. Fujimoto, P. Kienlen-Campard, S.N.
993 Constantinescu, J.N. Octave, S. Aimoto, and S.O. Smith. 2009b. A helix-
994 to-coil transition at the epsilon-cut site in the transmembrane dimer of the
995 amyloid precursor protein is required for proteolysis. *Proc Natl Acad Sci U*
996 *S A*. 106:1421-1426.
997 Scherthan, H., H. Wang, C. Adelfalk, E.J. White, C. Cowan, W.Z. Cande, and D.B.
998 Kaback. 2007. Chromosome mobility during meiotic prophase in
999 Saccharomyces cerevisiae. *Proc Natl Acad Sci U S A*. 104:16934-16939.
1000 Seoane, A.I., and D.O. Morgan. 2017. Firing of Replication Origins Frees Dbf4-
1001 Cdc7 to Target Eco1 for Destruction. *Current biology : CB*. 27:2849-
1002 2855.e2842.
1003 Sheehan, M.J., and W.P. Pawlowski. 2009. Live imaging of rapid chromosome
1004 movements in meiotic prophase I in maize. *Proc Natl Acad Sci U S A*.
1005 106:20989-20994.
1006 Shinohara, M., S.L. Gasior, D.K. Bishop, and A. Shinohara. 2000. Tid1/Rdh54
1007 promotes colocalization of rad51 and dmc1 during meiotic recombination.
1008 *Proceedings of the National Academy of Sciences of the United States of*
1009 *America*. 97:10814-10819.
1010 Shinohara, M., S.D. Oh, N. Hunter, and A. Shinohara. 2008. Crossover
1011 assurance and crossover interference are distinctly regulated by the ZMM
1012 proteins during yeast meiosis. *Nat Genet*. 40:299-309.
1013 Shinohara, M., E. Shita-Yamaguchi, J.M. Buerstedde, H. Shinagawa, H. Ogawa,
1014 and A. Shinohara. 1997. Characterization of the roles of the
1015 Saccharomyces cerevisiae RAD54 gene and a homologue of RAD54,
1016 RDH54/TID1, in mitosis and meiosis. *Genetics*. 147:1545-1556.

Smith, S.O., C. Smith, S. Shekar, O. Peersen, M. Ziliox, and S. Aimoto. 2002. Transmembrane interactions in the activation of the Neu receptor tyrosine kinase. *Biochemistry*. 41:9321-9332.

Sosa Ponce, M.L., S. Moradi-Fard, V. Zaremberg, and J.A. Cobb. 2020. SUNny Ways: The Role of the SUN-Domain Protein Mps3 Bridging Yeast Nuclear Organization and Lipid Homeostasis. *Frontiers in genetics*. 11:136.

Starr, D.A., and H.N. Fridolfsson. 2010. Interactions Between Nuclei and the Cytoskeleton Are Mediated by SUN-KASH Nuclear-Envelope Bridges. *Annu Rev Cell Dev Biol*.

Storlazzi, A., L. Xu, L. Cao, and N. Kleckner. 1995. Crossover and noncrossover recombination during meiosis: timing and pathway relationships. *Proc Natl Acad Sci U S A*. 92:8512-8516.

Storlazzi, A., L. Xu, A. Schwacha, and N. Kleckner. 1996. Synaptonemal complex (SC) component Zip1 plays a role in meiotic recombination independent of SC polymerization along the chromosomes. *Proceedings of the National Academy of Sciences of the United States of America*. 93:9043-9048.

Tagliabracci, V.S., J.L. Engel, J. Wen, S.E. Wiley, C.A. Worby, L.N. Kinch, J. Xiao, N.V. Grishin, and J.E. Dixon. 2012. Secreted kinase phosphorylates extracellular proteins that regulate biomineralization. *Science (New York, N.Y.)*. 336:1150-1153.

Tagliabracci, V.S., L.A. Pinna, and J.E. Dixon. 2013. Secreted protein kinases. *Trends in biochemical sciences*. 38:121-130.

Tagliabracci, V.S., S.E. Wiley, X. Guo, L.N. Kinch, E. Durrant, J. Wen, J. Xiao, J. Cui, K.B. Nguyen, J.L. Engel, J.J. Coon, N. Grishin, L.A. Pinna, D.J. Pagliarini, and J.E. Dixon. 2015. A Single Kinase Generates the Majority of the Secreted Phosphoproteome. *Cell*. 161:1619-1632.

Tamagaki, H., Y. Furukawa, R. Yamaguchi, H. Hojo, S. Aimoto, S.O. Smith, and T. Sato. 2014. Coupling of transmembrane helix orientation to membrane release of the juxtamembrane region in FGFR3. *Biochemistry*. 53:5000-5007.

Taxis, C., C. Maeder, S. Reber, N. Rathfelder, K. Miura, K. Greger, E.H. Stelzer, and M. Knop. 2006. Dynamic organization of the actin cytoskeleton during meiosis and spore formation in budding yeast. *Traffic*. 7:1628-1642.

1050 Trelles-Sticken, E., C. Adelfalk, J. Loidl, and H. Scherthan. 2005. Meiotic
1051 telomere clustering requires actin for its formation and cohesin for its
1052 resolution. *J Cell Biol*. 170:213-223.
1053 Trelles-Sticken, E., M.E. Dresser, and H. Scherthan. 2000. Meiotic telomere
1054 protein Ndj1p is required for meiosis-specific telomere distribution,
1055 bouquet formation and efficient homologue pairing. *J Cell Biol*. 151:95-106.
1056 Trelles-Sticken, E., J. Loidl, and H. Scherthan. 1999. Bouquet formation in
1057 budding yeast: initiation of recombination is not required for meiotic
1058 telomere clustering. *Journal of cell science*. 112 (Pt 5):651-658.
1059 Ubersax, J.A., E.L. Woodbury, P.N. Quang, M. Paraz, J.D. Blethrow, K. Shah,
1060 K.M. Shokat, and D.O. Morgan. 2003. Targets of the cyclin-dependent
1061 kinase Cdk1. *Nature*. 425:859-864.
1062 Wan, L., H. Niu, B. Futcher, C. Zhang, K.M. Shokat, S.J. Boulton, and N.M.
1063 Hollingsworth. 2008. Cdc28-Clb5 (CDK-S) and Cdc7-Dbf4 (DDK)
1064 collaborate to initiate meiotic recombination in yeast. *Genes &*
1065 *development*. 22:386-397.
1066 Wan, L., C. Zhang, K.M. Shokat, and N.M. Hollingsworth. 2006. Chemical
1067 inactivation of cdc7 kinase in budding yeast results in a reversible arrest
1068 that allows efficient cell synchronization prior to meiotic recombination.
1069 *Genetics*. 174:1767-1774.
1070 Wanat, J.J., K.P. Kim, R. Koszul, S. Zanders, B. Weiner, N. Kleckner, and E. Alani.
1071 2008. Csm4, in collaboration with Ndj1, mediates telomere-led
1072 chromosome dynamics and recombination during yeast meiosis. *PLoS*
1073 *genetics*. 4:e1000188.
1074 Xu, L., M. Ajimura, R. Padmore, C. Klein, and N. Kleckner. 1995. NDT80, a
1075 meiosis-specific gene required for exit from pachytene in Saccharomyces
1076 cerevisiae. *Mol Cell Biol*. 15:6572-6581.
1077 Zickler, D., and N. Kleckner. 1998. The leptotene-zygotene transition of meiosis.
1078 *Annu Rev Genet*. 32:619-697.
1079 Zickler, D., and N. Kleckner. 1999. Meiotic chromosomes: integrating structure
1080 and function. *Annu Rev Genet*. 33:603-754.
1081 Zuela, N., and Y. Gruenbaum. 2016. Matefin/SUN-1 Phosphorylation on Serine
1082 43 Is Mediated by CDK-1 and Required for Its Localization to Centrosomes

and Normal Mitosis in C. elegans Embryos. *Cells*. 5.

1085 **Figure legends**

1086

1087 **Figure 1. Meiotic Mps3 localization and movement on NEs**

1088 (A) Mps3-GFP localization was analyzed in wild-type cells (PRY64) at various
1089 time points during meiosis. Bottom color bars indicates classes of Mps3-
1090 localization in (B). Bar indicates 2 μm.

1091 (B) Based on Mps3-GFP localization, cells with Mps3-GFP were classified into
1092 four classes (A) and quantified: single Mps3 focus (blue), 2–5 foci (green),
1093 more than 5 foci/patches (orange), and coverage on NE (red). At each time
1094 point, more than 150 nuclei were counted.

1095 (C) Time-lapse analysis of Mps3-GFP in the wild-type strain (PRY64) at different
1096 time points in meiosis. A single focal plane of a cell was analyzed every 3 sec.

1097 (D) Time-lapse analysis of Mps3-GFP in various strains at different time points in
1098 meiosis. A single focal plane of a cell was analyzed every 3 sec. The inhibitor
1099 LatB (30 μM) was added at 0 h. While washing, the inhibitor was washed at
1100 5 h, and the cells were analyzed at 6 h. Wild type, PRY64; *ndj1*, PRY192;
1101 *csm4*, PRY198.

1102 (E) Time-lapse analysis of Mps3-GFP in the *cdc28-as1* mutant (PRY71) treated
1103 with or without the inhibitor 1NM-PP1 (0.5 μM) at 5 h during meiosis. The
1104 inhibitor was added at 0 h (second panels) or 3 h (third panels). While
1105 washing (fourth panels), the inhibitor was added at 0 h and washed at 3 h,
1106 and the cells were analyzed at 5 h. Time-lapse analysis of Mps3-GFP in the
1107 *cdc7-as3* mutant (PRY260) treated with or without the inhibitor PP1 (15 μM).
1108 The *cdc7 bob1-1* mutant (PRY115) was analyzed at 6 h.

1109 (F) Tracking of Mps3-GFP in wild type, *cdc28-as1* (PRY71 with the inhibitor),
1110 *cdc7-as3* (PRY260with the inhibitor), and *cdc7 bob1-1* (PRY115). Tracking
1111 was monitored for all Mps3 foci/patches in a single cell for 120 sec. Each line
1112 represents tracking of the foci at a single focal plane.

1113 (G) Whole-cell staining analysis of Mps3-Flag and Ndj1. Various cells were
1114 stained with anti-Flag for Mps3-Flag (red) and anti-HA for Ndj1 (green) at the
1115 nuclear periphery at indicated times. *cdc28-as1* (PRY13) and *cdc7-as3*
1116 (PRY72) cells were treated with their inhibitor from 0 h and examined at the
1117 indicated times. Wild type, HKY404.

1118

1119 **Figure 2. Meiotic telomere movement in *cdk* and *ddk* mutants**

1120 (A–C) Time-lapse analysis of Rap1-GFP in various strains (wild type [A; HKY167],
1121 *cdc28-as1* [B, PRY68], and *cdc7-as3* [C, PRY79] and *cdc7 bob1-1* [C,
1122 PRY116]) at different time points during meiosis. An image of a single focal
1123 plane of each mutant cell was taken every 3 sec. For the *cdc28-as1* and *cdc7-*
1124 *as3* mutants, the inhibitors (0.5 μM of 1NM-PP1 and 15 μM PP1, respectively)
1125 were added at 0 h (second panels) or 3 h (third panels). While washing
1126 (bottom panels), the inhibitor was added at 0 h and washed at 3 h, and the
1127 cells were analyzed at 5 h. Clustering of telomeres is shown by arrows. Bar
1128 indicates 2 μm.

1129 (D) Tracking of Rap1-GFP in wild type (0 and 4h), *cdc28-as1* (with the inhibitor),
1130 and *cdc7-as3* (with the inhibitor). Tracking was monitored for all Rap1 foci in
1131 a single cell for 120 sec. Each line represents tracking of the center of foci at
1132 a single focal plane. Red dotted lines indicate the rim of each nucleus.

1133 (E) Kinetics of telomere clustering during meiosis were quantified. At each time
1134 point, more than 150 nuclei were counted for clustering of telomeres (arrows).

1135

1136 **Figure 3. Mps3 is phosphorylated in luminal region**

1137 (A) Schematic representation of the Mps3 protein. The putative transmembrane
1138 (TM) region and SUN domain are shown in green and gray, respectively.

1139 (B) Sequence homology of an Mps3 region with a CDK/DDK phosphorylation site
1140 of the Mer2 protein. Identical amino acids are shown in red. Putative CDK or
1141 DDK phosphorylation sites are shown in yellow. The substitutions (*mps3-AAA,*
1142 *MPS3-DDD*, and *MPS3-MER2S*) for the putative phosphorylation sites of
1143 Mps3 are shown.

1144 (C) Western blotting of Mps3 and tubulin at various times in meiosis. Cell lysates
1145 from the *MPS3-Flag* (right, HKY404) and *MPS3-AAA-Flag* (left, PRY163)
1146 strains were analyzed by western blotting using anti-Flag and anti-tubulin
1147 antibodies. The wild-type Mps3 protein shows band shift during meiosis for
1148 example at 4 and 6 h.

1149 (D) Western blotting of the Mps3-Flag protein during meiosis. Wild-type (left,
1150 HKY404), *mps3-AAA* mutant (middle, PRY163) and *MPS3-MER2S* mutant

1151 proteins (right, PRY514) were analyzed at different time points. Fractions
1152 immunoprecipitated with anti-Flag antibody were probed with anti-Flag
1153 antibody (top) as well as a phospho-specific antibody (bottom) that
1154 recognized T189 and S190 phosphorylation.
1155 (E) Western blotting of the Mps3-Flag protein during meiosis. Wild-type (left,
1156 HKY404) and *MPS3-MER2s* proteins (right, PRY514) were analyzed at
1157 different time points. Fractions immunoprecipitated with anti-Flag antibody
1158 were probed with anti-Flag and anti-Mer2-phospho-S30 antibodies.
1159 (F, G) Rap1-GFP dynamics at 4 h of meiosis analyzed in *MPS3-MER2s* (PRY518)
1160 and wild-type (HKY167) strains. Kinetics of Rap1 clustering in each strain is
1161 shown in G. Counting was performed as described in Figure 2E. Blue, wild
1162 type; red, *MPS3-MER2S.*
1163 (G) Localization of Ndj1-HA (green), Mps3-Mer2S-Flag (red), and DAPI (dark
1164 blue) was analyzed by whole cell staining of PRY514. Bar indicates 2 μm.
1165
1166 **Figure 4. The *mps3-AAA* mutant impairs telomere and NE movement**
1167 (A) Meiosis division was analyzed by DAPI staining for various strains. More than
1168 100 cells were counted for divisions. Spore viability of each strain is shown in
1169 parenthesis. At least 100 asci were dissected for each strain.
1170 (B) Time-lapse analysis of Rap1-GFP in the wild-type (HKY167) and *mps3-AAA*
1171 (PRY138) strains at different time points in meiosis. A single focal plane of a
1172 cell was analyzed every 3 s. A tethering defect was observed in the *mps3-*
1173 *AAA* strains. Bar indicates 2 μm.
1174 (C) Tracking of Rap1-GFP in wild type (left) and *mps3-AAA*. See Figure 2E for
1175 quantification.
1176 (D) Time-lapse analysis of Zip1-GFP in wild type (SEY672) and *mps3-AAA*
1177 (PRY332).
1178 (E) Tracing of Zip1-GFP shows a step size of each Zip1-GFP line. Step size per
1179 given time is converted into the relative velocity of chromosomes. Blue bars;
1180 wild type; red bars, *mps3-AAA.*
1181 (F) Localization of wild-type Mps3-GFP (PRY64) and Mps3-AAA-GFP (PRY186)
1182 proteins in a cell at different time points in meiosis.
1183 (G) Kinetics of Mps3 distribution. Based on Mps3-GFP morphology, cells with

1184 Mps3-GFP were classified into four classes and quantified: 2–5 foci (green),
1185 more than 5 foci/patches (orange), and coverage on NE (red). See Figure 1B
1186 for quantification.
1187 (H) Time-lapse analysis of wild type and Mps3-AAA-GFP during meiosis.
1188 (I) Tracking of Mps3-GFP in wild type (left) and *mps3-AAA*. See Figure 1F for
1189 quantification.
1190 (J) The maximum sectional area of each nucleus was measured using the
1191 Velocity program. Each area of the 96 nuclei is ranked in the figure. Graphs
1192 for wild type and *mps3-AAA* at 0 and 4 h as well as wild type treated with LatB
1193 are shown.
1194 (K) Interaction of Mps3-Flag with Ndj1-HA and Csm4 in the *mps3-AAA* mutant
1195 was confirmed by immuno-precipitation using anti-Flag antibodies. IPed
1196 fractions of cells with Mps3-Flag (left, HKY404) or Mps3-AAA-Flag (right,
1197 PRY163) at each time point were probed with anti-Flag (top), anti-HA (middle)
1198 and anti-Csm4 antibodies.
1199
1200 **Figure 5. Acid amino acids in lumen of Mps3 allele can suppress CDK and**
1201 **DDK defects**
1202 (A) Time-lapse analysis of Rap1-GFP in a phosphomimetic allele of *MPS3*,
1203 *MPS3-DDD* (PRY211), with a different combination of *cdc28-as1* (PRY211),
1204 *cdc7-as3* (PRY301), and *cdc7 bob1-1* (PRY272) mutations in meiosis. A
1205 single focal plane of a cell was analyzed at every 3 s. Bar indicates 2 μm.
1206 (B) Kinetics of clustering of telomere as Rap1-clusters was studied in *cdc7-as3*
1207 (left, PRY309) and *cdc28-as1* (right, PRY303) in the presence of its specific
1208 inhibitors. Wild type (blue, HKY167) and *MPS3-DDD* (PRY236) with the allele
1209 was used.
1210 (C) Time-lapse analysis of Mps3-DDD-GFP with different mutant alleles and in
1211 treatment with a specific inhibitor at different time points in meiosis.
1212 (D) Kinetics of Mps3. Based on Mps3-GFP morphology, cells with Mps3-GFP
1213 were classified into four classes and quantified: single Mps3 focus (blue), 2–
1214 3 foci (green), 4–5 foci (orange), and more than 5 foci (red). See Figure 2B
1215 for quantification. Graphs for wild type, *cdc28-as1*, and *cdc7-as3* cells are the
1216 same as in Figure 2B.

1217 (E) Tracking of Mps3-GFP in wild type (left) and *mps3-AAA*. See Figure 2D for
1218 quantification.
1219
1220 **Figure 6. Biophysical analysis of JM region of Mps3**
1221 (A) Amino acid sequences of Mps3 peptides used. Amino acid sequence in
1222 transmembrane region is shown in green. Phosphorylated residues TSS and
1223 its derivative DDD are shown in red.
1224 (B) Fluorescence spectra from a synthetic liposome containing Alexa568-labelled
1225 WT-Mps3 (left) peptide and Mps3-DDD peptide (right) were measured in the
1226 presence of various concentrations of PIP_2.
1227 (C) Schematic illustration of the binding of Mps3-WT peptide (left) and Mps3-DDD
1228 peptide (right) to lipid bilayer with PIP_2. DDD residues may induce electric
1229 repulsion wither between the peptides or between the peptide and the
1230 membrane.
1231 (D) Snapshots from all-atom MD simulation trajectories for Mps3-WT peptide (left),
1232 Mps3-DDD peptide (center) and Mps3-WT peptide with phosphorylation
1233 (right).
1234
1235 **Figure 7. A model of regulation of Mps3 on NE during meiosis**
1236 During mitosis, Mps3 forms a non-canonical LINC complex with *cis*-membrane
1237 interaction with Mps2 as a component of the half bridge and SPIN (left). Upon the
1238 induction of meiosis, unknown factor(s) promotes the formation of Mps3 foci on
1239 NE. Then, the JM region of Mps3 is subject to non-canonical phosphorylation,
1240 which in turn weaken the binding of the JM to INM, probably by electric repulsion
1241 between the JM regions with negative charges and acid lipids. This process
1242 promotes the formation of canonical LINC complex with the *trans*-membrane
1243 configuration, in which Mps3 SUN domain binds to KASH domain of Mps2 and
1244 Csm4. Csm4 may promote a structural change of luminal region of Mps2. The N-
1245 terminal region of Mps3, which is located in nucleoplasm binds to a telomere-
1246 binding protein, Ndj1. During middle and late prophase I, Mps3 forms a large
1247 protein ensembles on NE, which is seen as a patch. Mps3 foci and patches are
1248 clustered on one area of NE during zygotene stage, which corresponds with
1249 telomere bouquet. The resolution of Mps3 clusters is promoted by CDK and DDK

activities. During mitosis, DDK and other factor(s) limits the NE localization of Mps3.

Figure 1. Rao et. al.

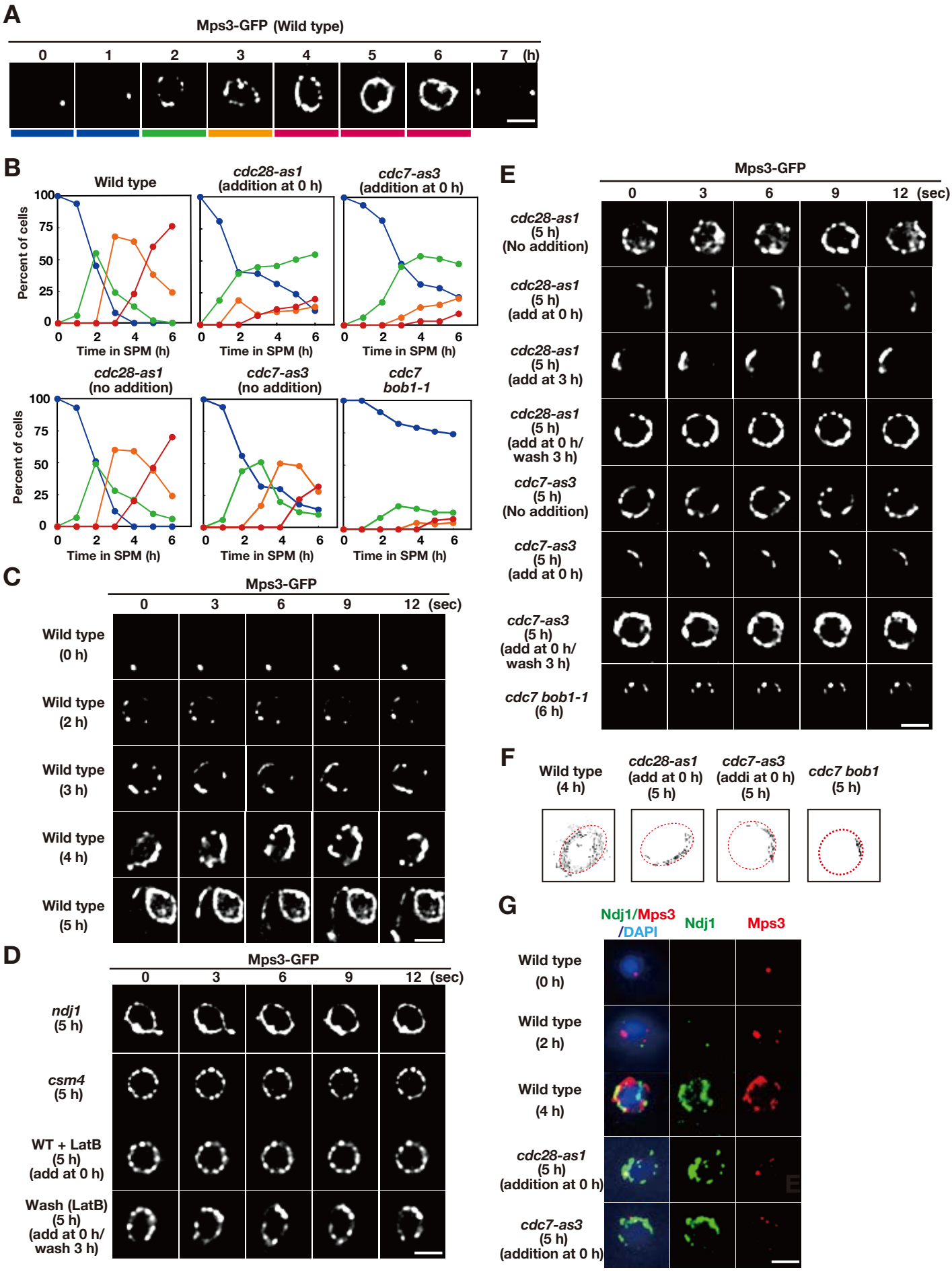

Figure 2. Rao et. al.

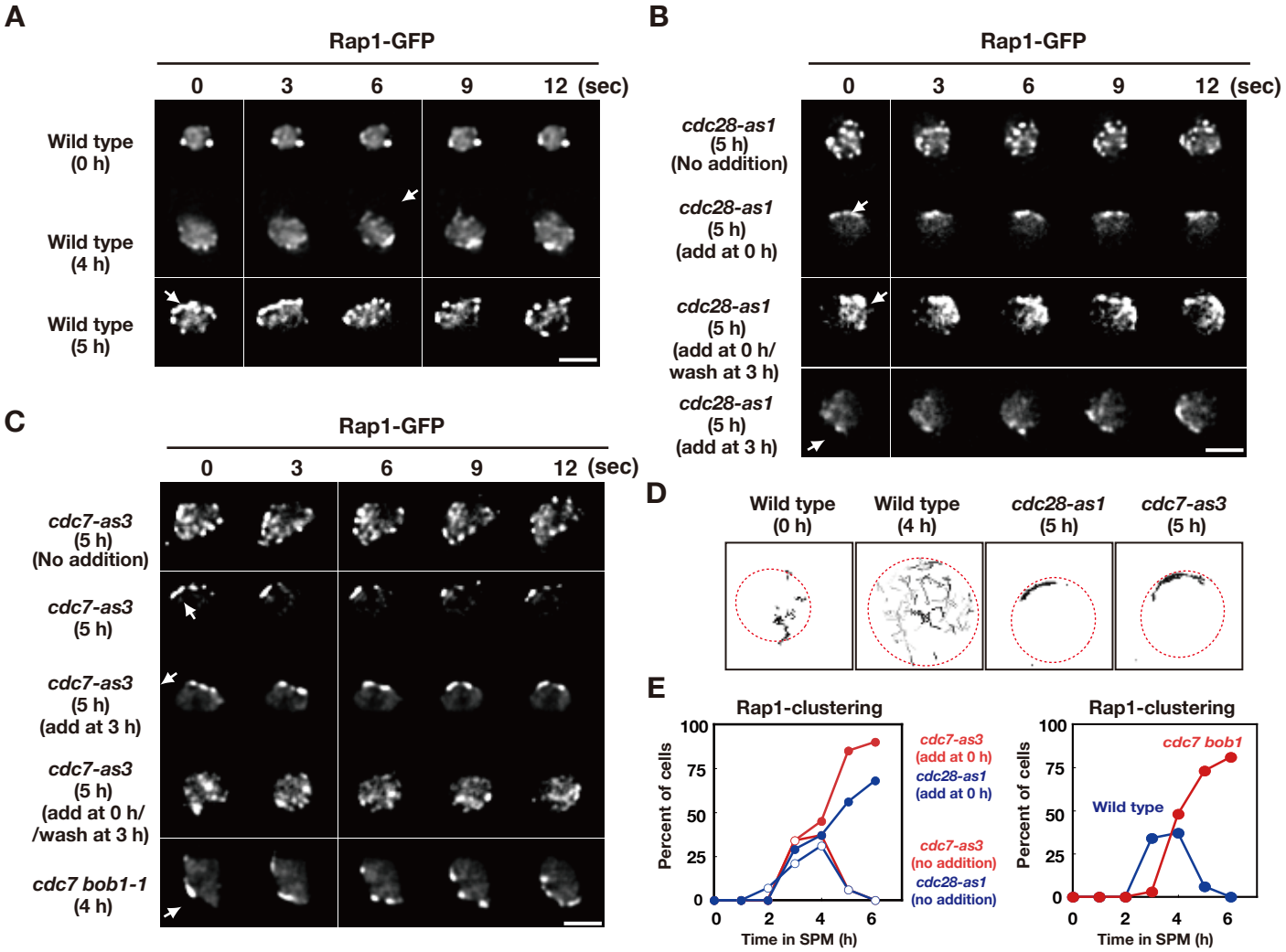

Figure 3 Rao et. al.

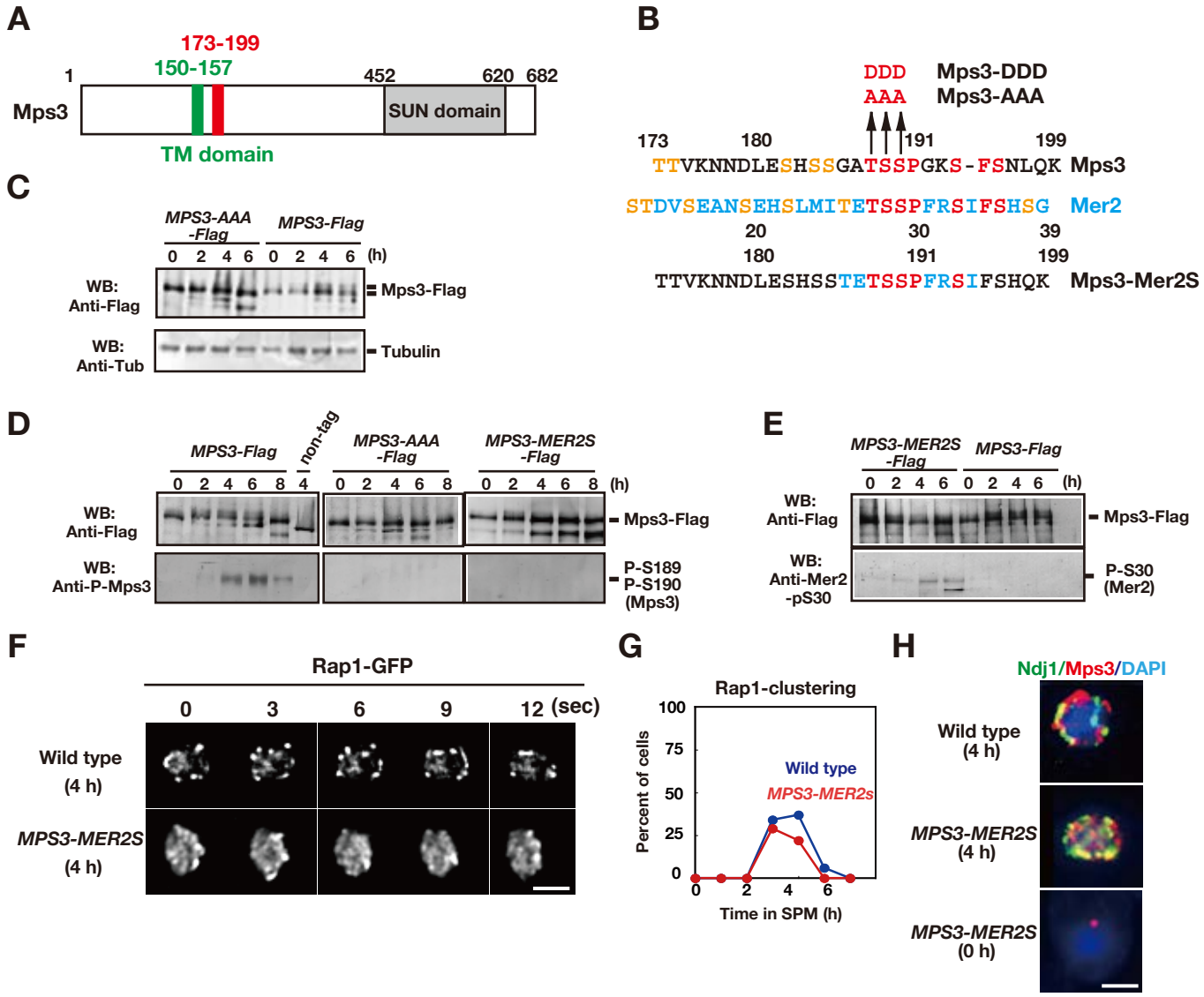

Figure 4 Rao et. al.

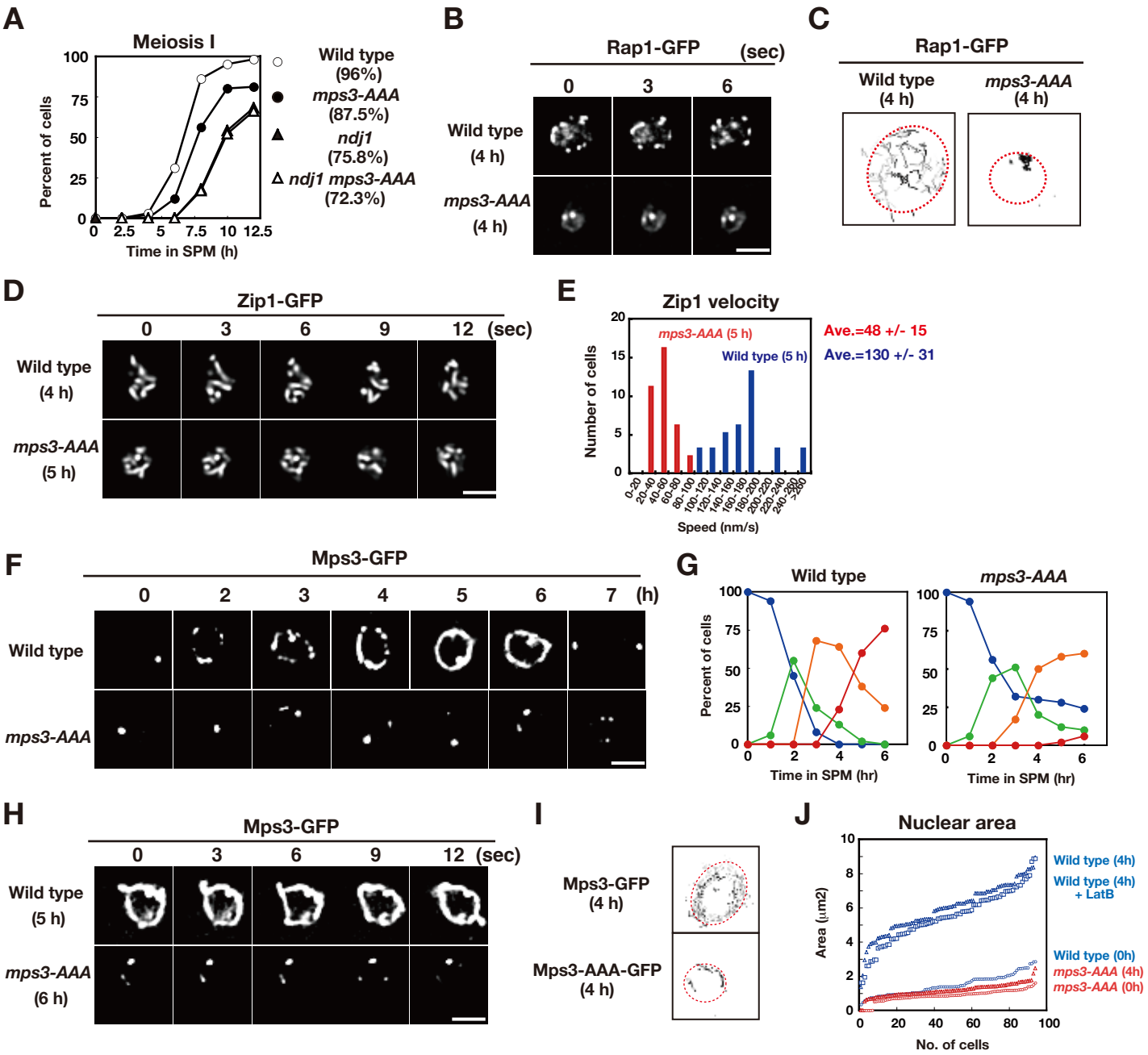

Figure 5 Rao et. al.

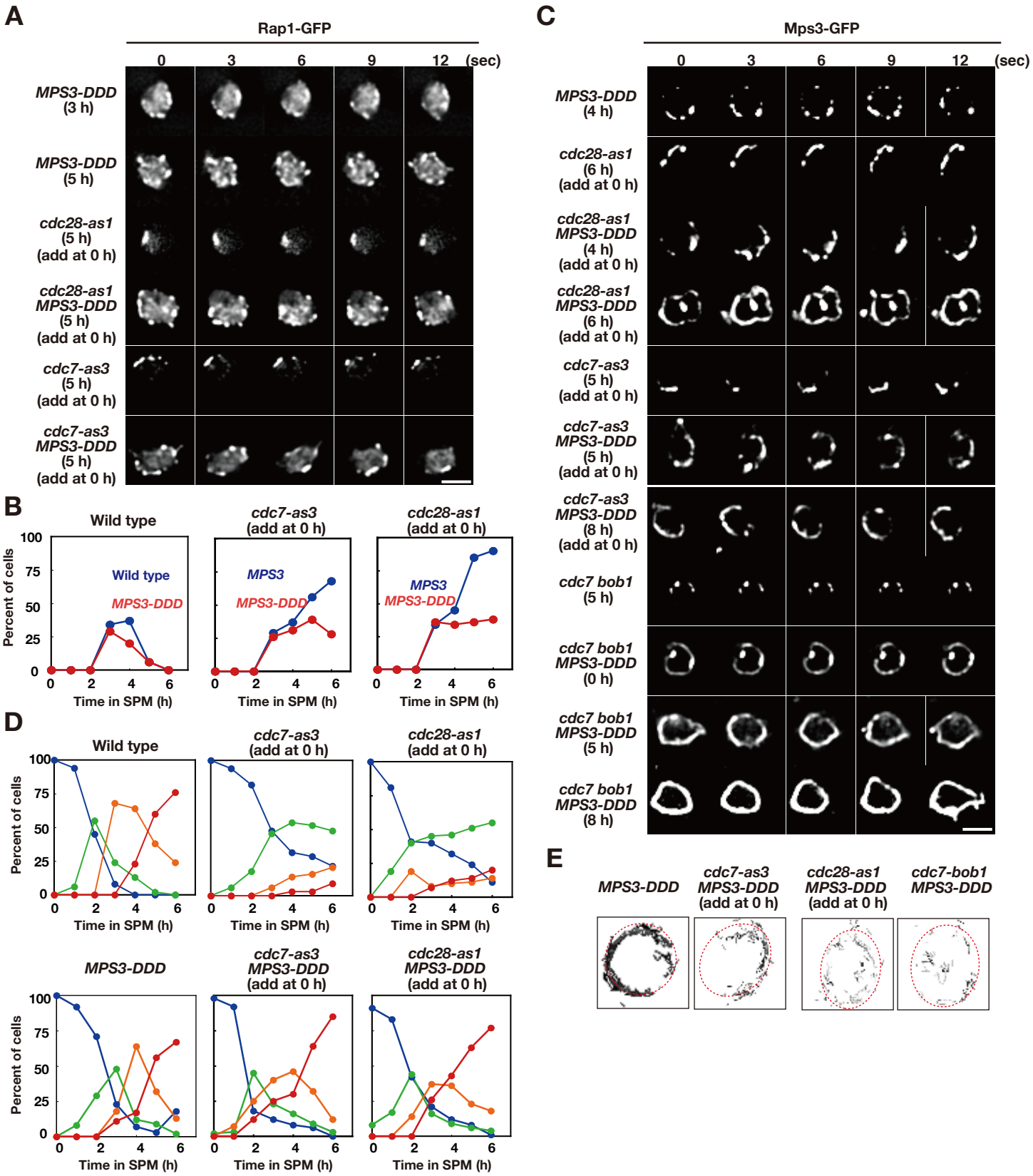

Figure 6. Rao et. al.

A

Mps3-WT NH2-GEAKKLKWRTYIFYGGLFFVFFFGSFLMTTVKNNDLESHSSGATSSPGKSFSNL

Mps3-DDD NH2-GEAKKLKWRTYIFYGGLFFVFFFGSFLMTTVKNNDLESHSSGADDDPGKSFSNL

B

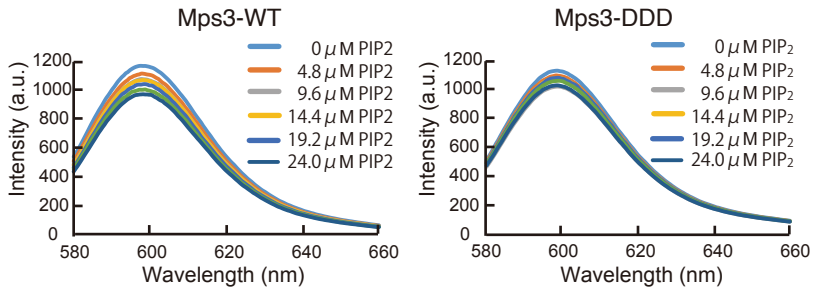

C

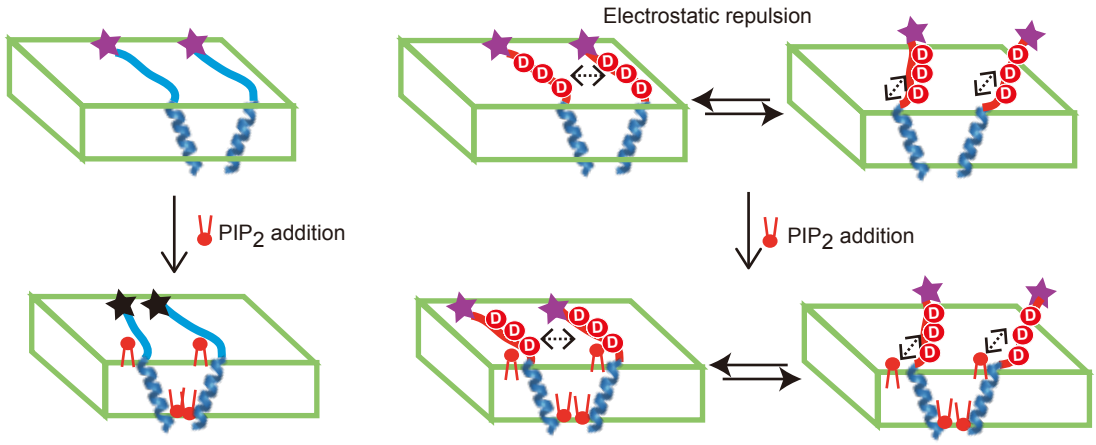

D

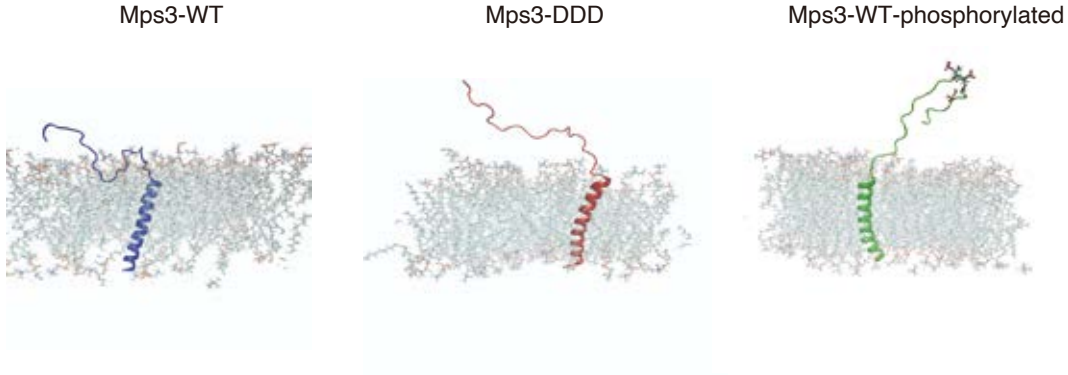

Figure 7 Rao et. al.

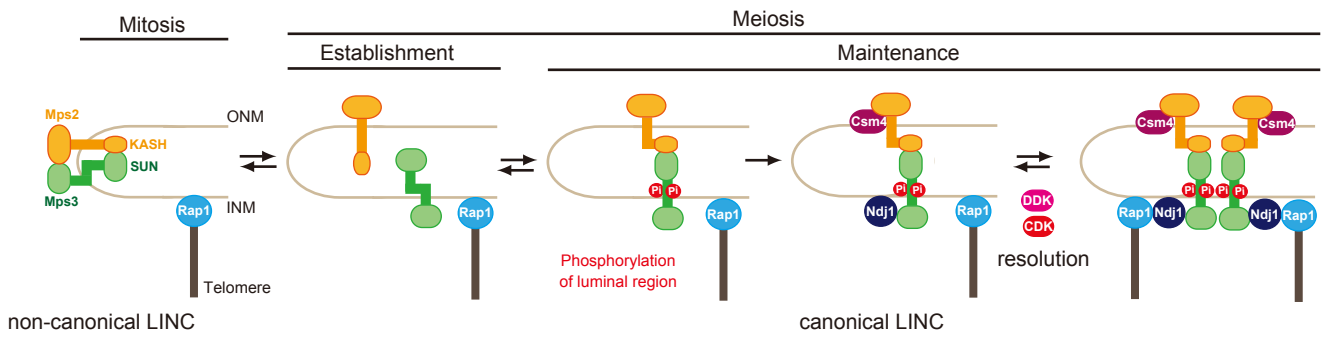

Supplemental information on Rao et al.

Supplemental Figure

Figure S1. Meiotic telomere movement in the presence of the inhibitors

(A) To check the off-target of two inhibitors, 1NM-PP1 (for *cdc28-as1*) and PP1 (for *cdc7-as3*), wild type diploid cells (HKY404) with Mps3-GFP were grown in the presence of each inhibitor (0.5 μM of 1NM-PP1, top panels; 15 μM PP1, bottom panels). The inhibitors were added at 0 h (second panels) and time-lapse images were examined in 4 h-incubation with SPM. The two inhibitors did not affect rapid movement of Mps3-GFP foci on NEs. Bar indicates 2 μm.

(B) Cytoplasmic actin cables were visualized by Phalloidin (red) and DAPI (purple) staining of *cdc28-as1* (PRY68) cells after 5 h of incubation in SPM both without (left) or with (middle) its inhibitor 1NM-PP1 from 0 h. As a control, the mutant cells were treated with 30 μM of latrunculin B (LatB) at 4 h and analysed for actin staining at 5 h (right). Bar indicates 2 μm.

(C) To check the off-target of two inhibitors, 1NM-PP1 (for *cdc28-as1*) and PP1 (for *cdc7-as3*), wild type diploid cells with Rap1-GFP were grown in the presence of each inhibitor (0.5 μM of 1NM-PP1, top panels; 15 μM PP1, bottom panels). The inhibitors were added at 0 h (second panels) and time-lapse images were examined in 4 h-incubation with SPM. The two inhibitors did not affect rapid movement of Rap1-GFP foci on NEs. Bar indicates 2 μm.

Figure S2. CDK and DDK are necessary for Mps3 localization on NE

(A) Schematic representation of the Mps3 protein. Five CDK consensus sequences are shown by red lines. The putative transmembrane (TM) region and SUN domain are shown in blue and gray, respectively.

(B) *In vivo* phosphorylation was confirmed by a decreased band shift of Mps3-Flag protein purified from meiotic cell lysates (4 h incubation with SPM) using the anti-Flag antibody. After immuno-precipitation, the precipitate was incubated with 1 unit of CIP for one hour either in the presence or absence of phosphatase inhibitors. Mps3-Flag was detected using anti-Flag (M2) antibody.

(C) Affinity-purified-Mps3-Flag from meiotic cell (HKY407) lysates (4 h incubation

1286 with SPM) using anti-Flag column was treated with CIP as described in (B)
1287 and was probed with anti-Phospho-Serine antibody (Qiagen). During
1288 incubation, Mps3 protein was degraded extensively (bottom).
1289 (D) Reactivity of wild-type Mps3-Flag and Mps3-AAA mutant protein to anti-
1290 phospho-serine antibody was examined by Western blotting. Wild-type Mps3-
1291 Flag and Mps3-AAA mutant protein at each time point were IPed and probed
1292 with the antibody. While wild-type Mps3-Flag shows an increase reactivity to
1293 the antibody, Mps3-AAA-Flag did not increase the reactivity in meiosis (4 h)
1294 compared to mitosis (0 h).
1295 (E) *In vitro* phosphorylation analysis of GST-Mps3 fusion proteins. Purified wild-
1296 type GST-Mps3 and GST-Mps3-AAA fragments (shown on the left by
1297 Coomassie staining) were incubated with different combinations of purified
1298 the Cdc28–Clb5 complex and/or Cdc7–Dbf4 kinase complexes in the
1299 presence of γ-^{32}P-ATP. After 1-h incubation, proteins were fractionated on a
1300 SDS-PAGE gel and analyzed using a phosphorimager for incorporation of ^{32}P
1301 in the Mps3 fragments (right bottom) and Cdc28/Cdc7 protein (right top). Cdc7
1302 was phosphorylated by CDK. Quantification is shown below the
1303 autoradiogram.
1304
1305 **Figure S3. Meiotic phenotypes of *mps3-AAA* and *MPS3-DDD* mutants**
1306 (A) Whole cell staining of Mps3-Flag and Tubulin. Wild type (MSY832/833) and
1307 the *mps3-AAA* mutant (PRY122) cells in mitosis were stained with anti-Flag
1308 (red) and anti-tubulin (green). Representative images with short spindles with
1309 two Mps3 foci are shown. Bar indicates 2 μm.
1310 (B) FACS analysis of DNA contents in wild type and the *mps3-AAA* mutant cells
1311 at indicated times. Cells at each time point were fixed and stained with
1312 propidium iodide (PI) and analyzed by FACS after the sonication.
1313 (C) Immunostaining analysis of meiotic chromosome proteins. For SC formation,
1314 Zip1 localization (red) with DAPI (blue) image is also analyzed for wild type
1315 (top) and *mps3-AAA* mutant strains (bottom) at 4 h.
1316 (D) Kinetics of SC formation. SC elongation was analyzed by staining Zip1 protein.
1317 Class I (blue) contains Zip1 dots, Class II (green) contains partial lines of Zip1,
1318 and Class III (red) contains fully elongated Zip1 lines.

1319 (E) Localization of Red1 (green) and Hop1 (red) was analyzed in the wild type
1320 (top) and *mps3-AAA* mutant (bottom) at 4 h. Bars indicate 1 μm.
1321 (F) Meiosis division was analyzed by DAPI staining for wild type and the *MPS3-*
1322 *DDD* strains (PRY201).
1323 (G) Localization of Mps3-DDD-GFP protein in wild type (PRY211) at different time
1324 points. Bar indicates 2 μm.
1325 (H) Localization of Mps3-DDD-GFP protein in wild type, *cdc28-as1* (with 1NM-
1326 PP1; PRY301) and *cdc7-as3* (with PP1; PRY272) at 0 h. Bar indicates 2 μm.
1327 (I) Time-lapse analysis of Rap1-GFP in the *mps3-DDD* strains with a different
1328 combination of *cdc28-as1*, *cdc7-as3* or *cdc7 bob1-1* mutations in mitosis (0
1329 h). A single-focal plane of a cell was analyzed at every 3 second. Bar indicates
1330 2 μm.
1331
1332 **Figure S4. Structure and dynamics of JM region of Mps3**
1333 (A) Polarized attenuated total reflection FT-IR spectra are shown. Spectra (red)
1334 a synthetic liposome containing Mps3-WT (left) peptide and Mps3-DDD
1335 peptide (right) were obtained with light polarized parallel (top) or
1336 perpendicular (bottom). Deconvoluted spectra into α-helix and β-sheet are
1337 shown in blue.
1338 (B) Snapshots from coarse-grained MD simulation trajectories for Mps3-WT
1339 peptide (left), Mps3-DDD peptide (right).
1340 (C) Mass density profiles relative to the center of the lipid bilayer for residues,
1341 T197, S198 and S199 on Mps3-WT peptide (blue), Mps3-DDD peptide (red)
1342 and Mps3-WT peptide with phosphorylation (green). Density profile for
1343 phosphate groups on lipids are colored with yellow.
1344
1345

1346 **Table S1: Strain list**

Strain Name	Genotype
NKY1551	*MAT**a**/α, ho::LYS2/", lys2/", leu2::hisG/", ura3/", his4B-LEU2/his4X-LEU2-URA3, arg4-bgl/arg4-nsp*
MSY832/833	*MAT**a**/α, ho::LYS2/", ura3/", leu2::hisG/", trp1::hisG/", lys2/"*
HKY404	*MAT**a**/α, ho::LYS2/", lys2/", leu2::hisG/", ura3/", MPS3-3FLAG::KanMX6/", NDJ1-3HA::KanMX6/ "*
PRY13	*MAT**a**/α, ho::LYS2/", lys2/", leu2::hisG/", ura3/", MPS3-3FLAG::KanMX6/", NDJ1-3HA::KanMX6/", cdc28-as1/"*
PRY72	*MAT**a**/α, ho::LYS2/", lys2/", leu2::hisG/", ura3/", MPS3-3FLAG::KanMX6/", NDJ1-3HA::KanMX6/",cdc7-as3-9MYC/"*
PRY 64	*MAT**a**/α, ho::LYS2/", lys2/", leu2::hisG/", ura3/", MPS3-3GFP::KanMX6/"*
PRY71	*MAT**a**/α, ho::LYS2/", lys2/", leu2::hisG/", ura3/", MPS3-3GFP::KanMX6/", cdc28-as1/"*
PRY260	*MAT**a**/α, ho::LYS2/", lys2/", leu2::hisG/", ura3/", MPS3-3GFP::KanMX6/", cdc7-as3-9MYC/"*
PRY115	*MAT**a**/α, ho::LYS2/", lys2/", leu2::hisG/", ura3/", MPS3-3GFP::KanMX6/", cdc7::KanMX6/", bob1-1/"*
PRY122	*MAT**a**/α, ho::LYS2/", lys2/", leu2::hisG/", ura3/", mps3-T188,S189A,S190A-PSTI/"*
PRY186	*MAT**a**/α, ho::LYS2/", lys2/", leu2::hisG/", ura3/", mps3-T188,S189A,S190A-PSTI-3GFP::KanMX6 /"*
PRY163	*MAT**a**/α, ho::LYS2/", lys2/", leu2::hisG/", ura3/", mps3-T188,S189A,S190A-PSTI-3FLAG::KanMX6 /", NDJ1-3HA::KanMX6/"*
PRY138	*MAT**a**/α, ho::LYS2/", lys2/", leu2::hisG/", ura3/", mps3-T188,S189A,S190A-PSTI/", Rap1-GFP::LEU2/"*
PRY201	*MAT**a**/α, ho::LYS2/", lys2/", leu2::hisG/", ura3/", mps3-T188D,S189D,S190D-BSPEI/"*
PRY211	*MAT**a**/α, ho::LYS2/", lys2/", leu2::hisG/", ura3/", mps3-T188D,S189D,S190D-BSPEI-3GFP::KanMX6/"*

PRY219	*MAT**a**/α, ho::LYS2/", lys2/", leu2::hisG/", ura3/", mps3-T188D,S189D,S190D-BSPEI-3FLAG::KanMX6/" NDJ1-3HA::KanMX6/"*
PRY236	*MAT**a**/α, ho::LYS2/", lys2/", leu2::hisG/", ura3/", mps3-T188D,S189D,S190D-BSPEI-3GFP::KanMX6/", Rap1-GFP::LEU2/"*
PRY301	*MAT**a**/α, ho::LYS2/", lys2/", leu2::hisG/", ura3/", mps3-T188D,S189D,S190D-BSPEI-3GFP::KanMX6/", cdc28-as1/"*
PRY272	*MAT**a**/α, ho::LYS2/", lys2/", leu2::hisG/", ura3/", mps3-T188D,S189D,S190D-BSPEI-3GFP::KanMX6/", cdc7-as3::9MYC/"*
HKY167	*MAT**a**/α, ho::LYS2/", lys2/", leu2::hisG/", ura3/", Rap1-GFP::LEU2/"*
PRY68	*MAT**a**/ α, ho::LYS2/", lys2/", leu2::hisG/", ura3/",, Rap1-GFP::LEU2/", cdc28-as1/"*
PRY79	*MAT**a**/α, ho::LYS2/", lys2/", leu2::hisG/", ura3/",, Rap1-GFP::LEU2/", cdc7-as3::9MYC/"*
PRY116	*MAT**a**/α, ho::LYS2/", lys2/", leu2::hisG/", ura3/",, Rap1-GFP::LEU2/", cdc7::KanMX6/", bob1-1/"*
PRY303	*MAT**a**/α, ho::LYS2/", lys2/", leu2::hisG/", ura3/", mps3-T188D,S189D,S190D-BSPEI/", Rap1-GFP::LEU2/", cdc28-as1/ "*
PRY309	*MAT**a**/α, ho::LYS2/", lys2/", leu2::hisG/", ura3/", mps3-T188D,S189D,S190D-BSPEI/", Rap1-GFP::LEU2/", cdc7-as3::9MYC/"*
PRY322	*MAT**a**/α, ho::LYS2/", lys2/", leu2::hisG/", ura3/", mps3-T188D,S189D,S190D-BSPEI/", Rap1-GFP::LEU2/", cdc7::KanMX6/", bob1-1/"*
PRY344	*MAT**a**/α, ho::LYS2/", lys2/", leu2::hisG/", ura3/", his4B-LEU2/his4X-LEU2-URA3, arg4-bgl/arg4-nsp, mps3-T188,S189A,S190A-PSTI/" rad50S::URA3/rad50S::URA3*
PRY192	*MAT**a**/α, ho::LYS2/", lys2/", leu2::hisG/", ura3/", MPS3-*

	3GFP::KanMX6/", ndj1::KanMX6/"
PRY198	*MAT**a**/α, ho::LYS2/", lys2/", leu2::hisG/", ura3/", MPS3-3GFP::KanMX6/", csm4::KanMX6/"*
PRY514	*MAT**a**/α, ho::LYS2/", lys2/", leu2::hisG/", ura3/", Mer2-Mps3 (swap)-SacI FLAG::KanMX6/", Rap1-GFP::LEU2/", NDJ1-HA/"*
SEY672	*MAT**a**/α, ho::LYS2/", lys2/", leu2::hisG/", ura3/", trp1::hisG/", ZIP1-GFP::KamMX6/"*
PRY332	*MAT**a**/α, ho::LYS2/", lys2/", leu2::hisG/", ura3/", trp1::hisG/", ZIP1-GFP::KamMX6/", mps3-T188,S189A,S190A-PSTI-3GFP::KanMX6 /"*
PRY311	*MAT**a**/α, ho::LYS2/", lys2/", leu2::hisG/", ura3/", lys2/", his4B-LEU2/his4X-LEU2-URA3, arg4-bgl/arg4-nsp, mps3-T188,S189A,S190A-PSTI /"*
PRY147	*MAT**a**/α, ho::LYS2/", lys2/", leu2::hisG/", ura3/", mps3-T188,S189A,S190A-PSTI /", ndj1::KamMX6/ ndj1::KamMX6*
HKY329	*MAT**a**/α, ho::LYS2/", lys2/", leu2::hisG/", ura3/", trp1::hisG/", his4B-LEU2/his4X-LEU2-URA3, arg4-bgl/arg4-nsp, ndj1::KamMX6/"*

1347

Supplemental Figure S1 Rao et. al.

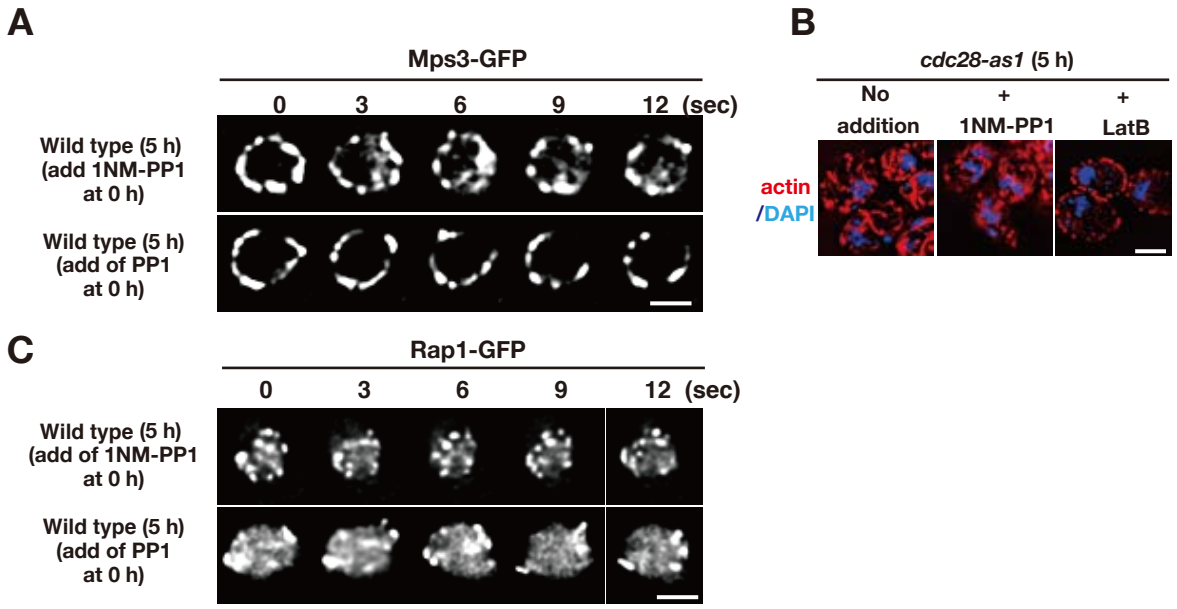

Supplemental Figure S2 Rao et. al.

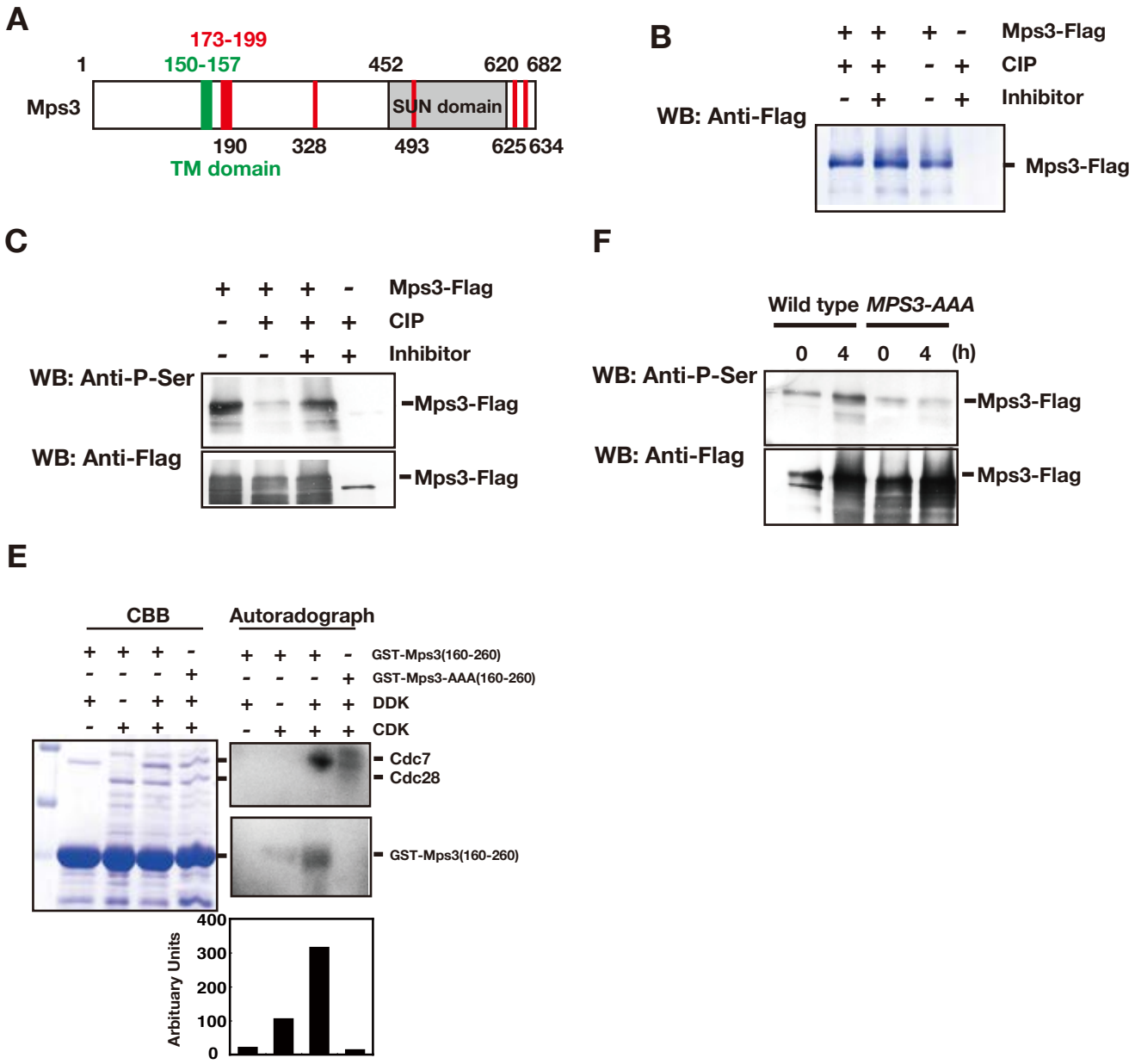

Supplemental Figure S3 Rao et. al.

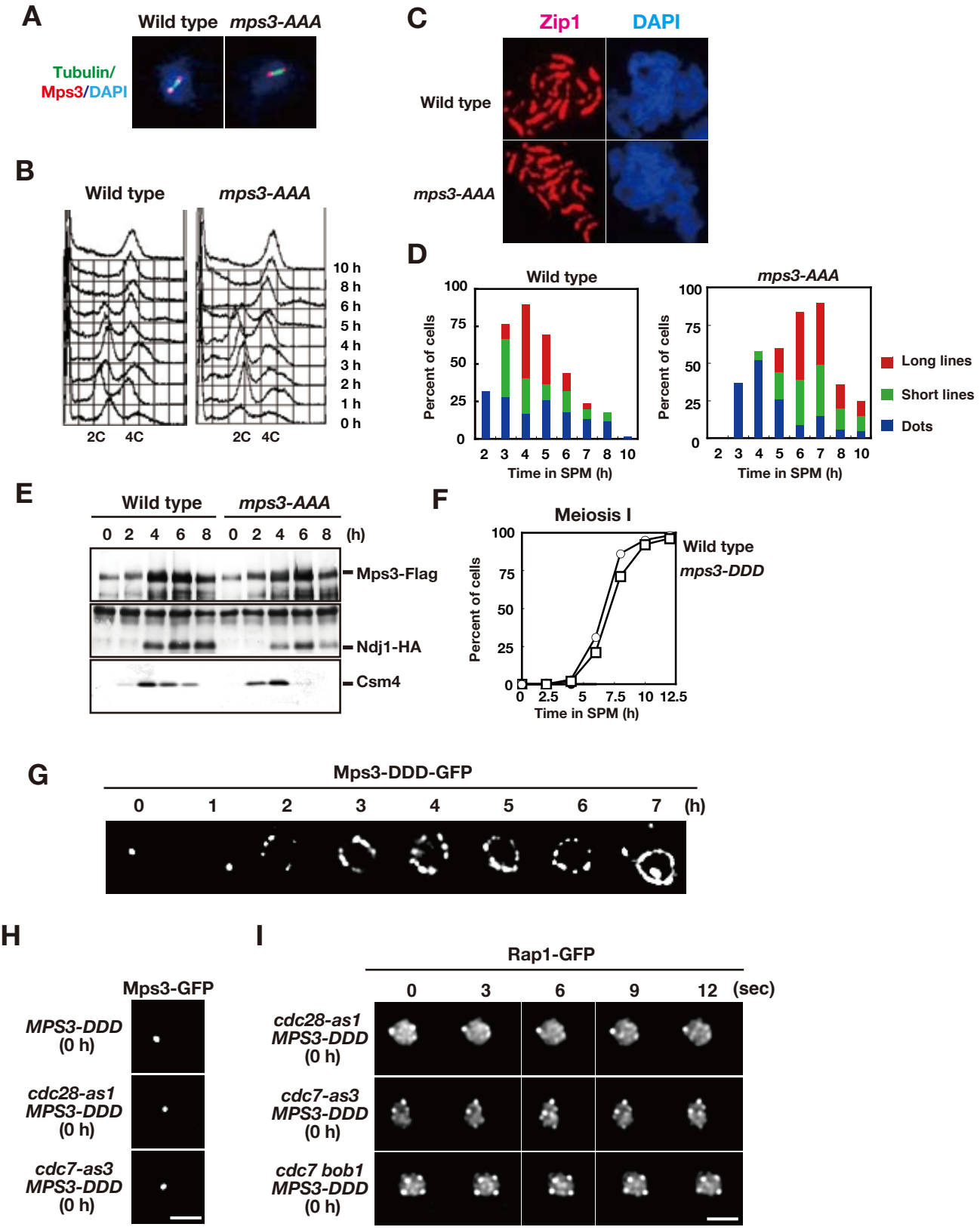
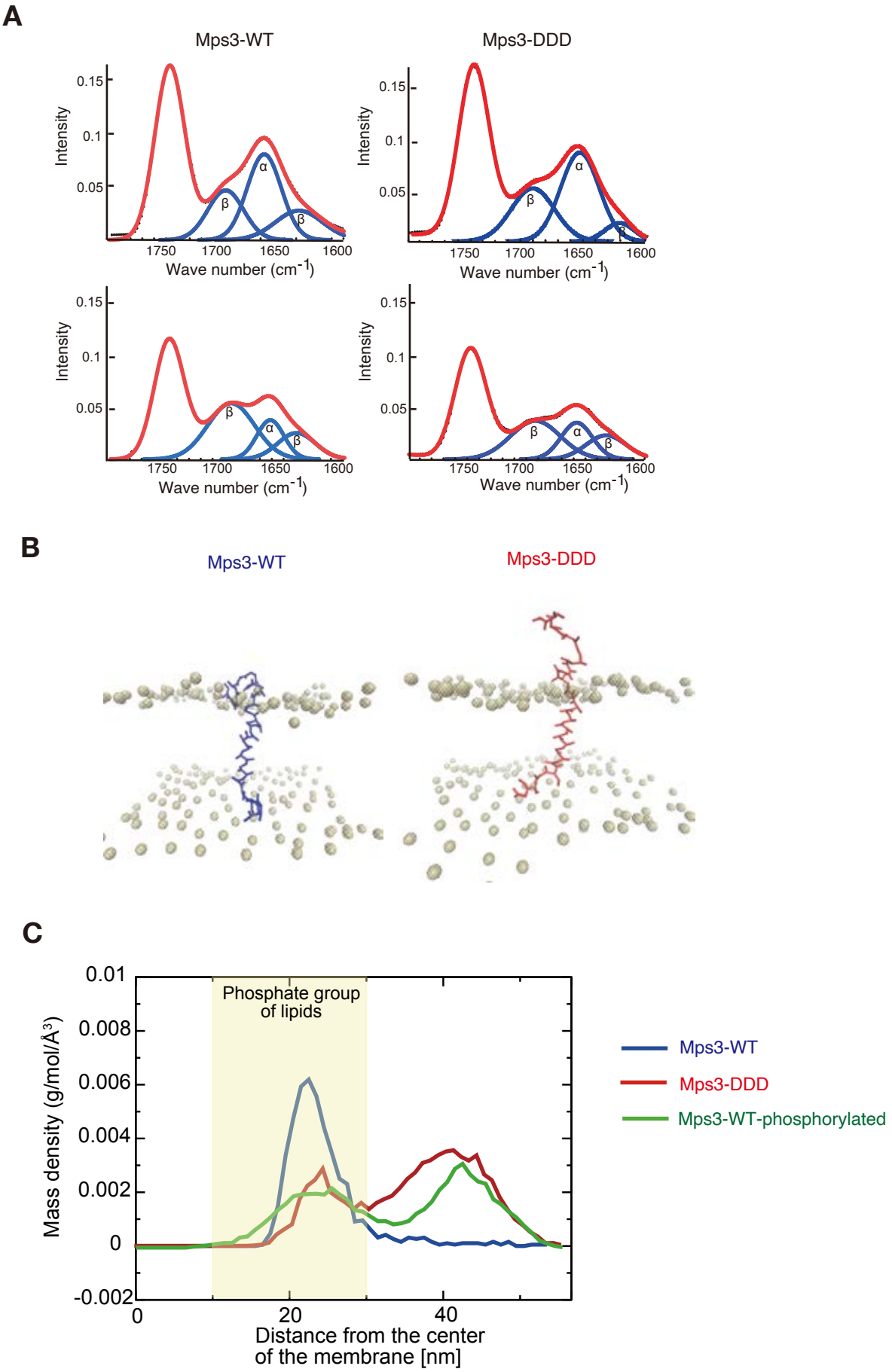
Supplemental Figure S4 Rao et. al.